JACS
JOURNAL OF THE AMERICAN CHEMICAL SOCIETY



Article

# Encoding multiple reactivity modes within a single synthetic replicator

Craig C. Robertson, Tamara Kosikova, and Douglas Philp

*J. Am. Chem. Soc.*, **Just Accepted Manuscript** • DOI: 10.1021/jacs.0c03527 • Publication Date (Web): 15 May 2020



is published by the American Chemical Society. 1155 Sixteenth Street N.W., Washington, DC 20036

*Journal of the American Chemical Society*

# Encoding multiple reactivity modes within a single synthetic replicator

Craig C. Robertson,[1,†] Tamara Kosikova,[1,2] and Douglas Philp[1,2,*]

[1]*School of Chemistry and EaStCHEM, University of St Andrews, North Haugh, St Andrews, Fife KY16 9ST, United Kingdom*

[2]*Department of Chemistry, Northwestern University, 2145 Sheridan Road, Evanston, Illinois 60208-3113, United States*

**Abstract:** Establishing instructable and self-sustaining replication networks in pools of chemical reagents is a key challenge in systems chemistry. Self-replicating templates are formed from two constituent components with complementary recognition and reactive sites *via* a slow bimolecular pathway and a fast template-directed pathway. Here, we re-engineer one of the components of a synthetic replicator to encode an additional recognition function, permitting the assembly of a binary complex between the components that mediates replicator formation through a template-independent pathway, which achieves maximum rate acceleration at early time points in the replication process. The complementarity between recognition sites creates a key conformational equilibrium between the catalytically inert product, formed *via* the template-independent pathway, and the catalytically active replicator that mediates the template-directed pathway. Consequently, the rapid formation of the catalytically inert isomer "kickstarts" replication through the template-directed pathway. Through kinetic analyses, we demonstrate that the presence of the two recognition-mediated reactivity modes results in enhanced template formation in comparison to systems capable of exploiting only a single recognition-mediated pathway. Finally, kinetic simulations reveal that the conformational equilibrium and both the relative and absolute efficiencies of the recognition-mediated pathways affect the extent to which self-replicating systems can benefit from this additional template-independent reactivity mode. These results allow us to formulate the rules that govern the coupling of replication processes to alternative recognition-mediated reactivity modes. The interplay between template-directed and template-independent pathways for replicator formation has significant relevance to ongoing efforts to design instructable and adaptable replicator networks.

## Introduction

Replication is a ubiquitous process in biological systems that ensures the faithful transmission of critical genetic information encoded in nucleic acids to their molecular progeny. On the prebiotic Earth, replication is believed to have played a key role in facilitating the transition[1] from a purely chemical world to one with emergent complexity—including life. Although the importance of replication processes in the context of origin of life scenarios is generally recognized, the specific nature of the first entity capable of information transfer and amplification through a replicative mechanism remains a source of significant ongoing debate.[2] A key objective of systems chemistry[2b,3] is to move beyond the limitations and challenges associated with the study of molecules with specific relevance to either prebiotic chemistry or extant biology in order to develop a better understanding of the principles that govern the appearance of complex function, including replication, in synthetic systems. Following a body of work focused[4] on the template-directed synthesis of oligonucleotides, in 1986 von Kiedrowski described[5] the first example of an artificial replicating system capable of catalyzing its own formation. Since then, minimal replicating systems[6] have been designed using a range of chemistries—from oligonucleotides[5,7] and peptides[8] to small organic molecules[9]—demonstrating that replication is possible even in the absence of intricate enzymatic machinery. Some of these minimal replicating systems have also been incorporated[10–12] into reaction networks in which several interconnected replicators operate simultaneously.

In the minimal[6] model of self-replication (Figure 1, left), two components—**A** and **B1**—are equipped with complementary recognition and reactive sites. The reaction between **A** and **B1** proceeds initially through a slow bimolecular pathway, generating template $\mathbf{T^{AB1}}$, which bears both of the recognition sites (Figure 1, gray and green) derived from the starting building blocks. Consequently, once formed, template $\mathbf{T^{AB1}}$ can associate with unreacted **A** and **B1** affording a catalytically active ternary complex [$\mathbf{A{\bullet}B1{\bullet}T^{AB1}}$], in which the reactive sites in **A** and **B1** (Figure 1, blue and orange) are preorganized for reaction. In this manner, $\mathbf{T^{AB1}}$ can serve as a template for its own formation. The rate of formation of template $\mathbf{T^{AB1}}$ is correlated directly with the concentration of the reactive ternary complex [$\mathbf{A{\bullet}B1{\bullet}T^{AB1}}$], which, in turn, depends on the relative strengths of the association between $\mathbf{T^{AB1}}$ and its constituent components **A** and **B1**, as well as the stability of the [$\mathbf{T^{AB1}{\bullet}T^{AB1}}$] homodimer. Therefore, in a scenario where the two building blocks **A** and **B1** react in the absence of preformed template, the kinetic profile can exhibit a lag period (Figure 1, bottom left) in product formation at early time points in the reaction. The presence of this lag period is a direct consequence of the

reliance of the system on the slow bimolecular pathway for the formation of $\mathbf{T}^{\mathbf{AB1}}$ in the initial stages of the reaction. Consequently, the addition of preformed template $\mathbf{T}^{\mathbf{AB1}}$ to a solution of **A** and **B1** at $t = 0$ acts as an instruction to the system to form additional $\mathbf{T}^{\mathbf{AB1}}$ and would be expected to result in a reduction or disappearance of the lag period. For this reason, kinetic experiments employing pre-formed template as instruction are key to demonstrating the ability of these systems to template their own formation.

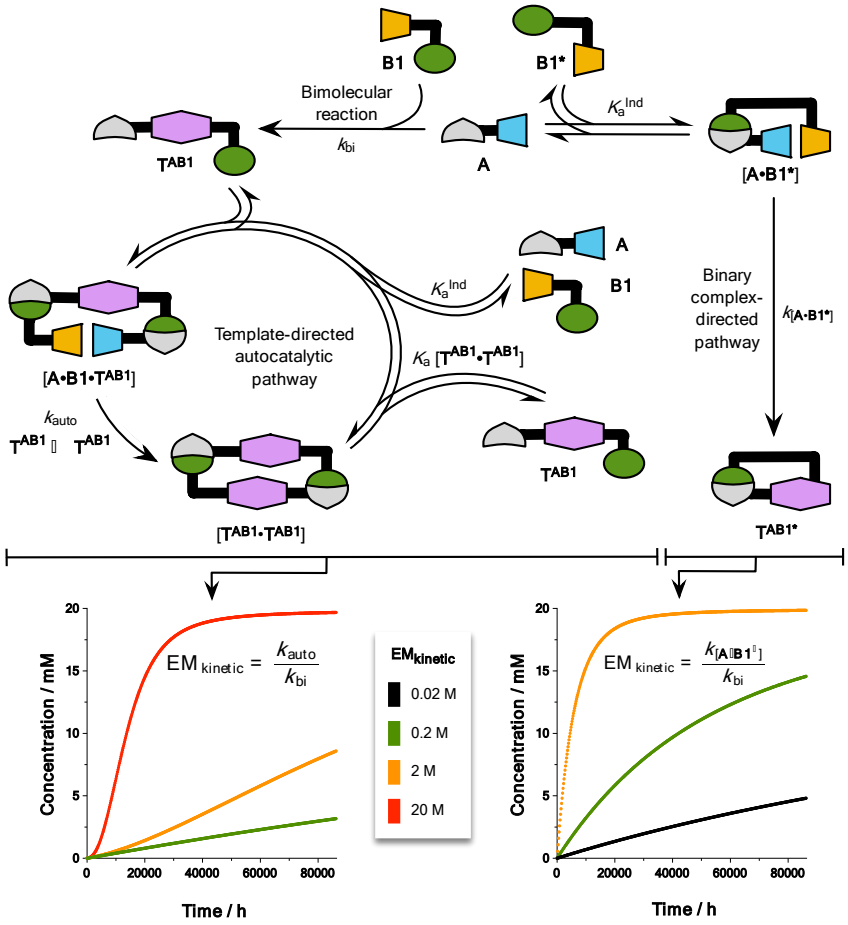


**Figure 1.** Cartoon representation of the minimal model of self-replication, where components **A** and **B1** are equipped with complementary recognition (gray/green) and reactive (blue/orange) sites. Components **A** and **B1** react *via* a slow bimolecular reaction to form template $\mathbf{T}^{\mathbf{AB1}}$. Once formed, $\mathbf{T}^{\mathbf{AB1}}$ is capable of directing its own formation by assembling **A** and **B1** into catalytically active ternary complex [**A•B1•T**$^{\mathbf{AB1}}$]. An alternative to the template-directed self-replication pathway is the reaction between two components bearing complementary reactive and recognition sites—for example, **A** with **B1***—which can be accelerated by the formation of binary complex [**A•B1***], leading to catalytically-inert template $\mathbf{T}^{\mathbf{AB1*}}$. The effective kinetic molarity ($EM_{kinetic}$) affects the time–course profiles of systems capable of (bottom left) template-directed self-replication and (bottom right) reaction through the [**A•B1***] binary complex. Simulated conditions: [**A**] = [**B1**] or [**B1***] = 20 mM, $k_{bi} = 1 \times 10^{-4}$ M$^{-1}$ s$^{-1}$, $K_a^{Ind} = 10^3$ M$^{-1}$, $K_a^{Duplex} = 10^6$ M$^{-1}$; see the Supporting Information for example scripts.

In addition to the direct catalysis of the reaction between **A** and **B1** by template $\mathbf{T}^{\mathbf{AB1}}$, the reaction between two appropriately-designed components can also be accelerated[9e,13] in a template-independent manner through the formation of a binary complex (Figure 1). In this

case, two components—**A** and **B1***—associate together to give binary complex [**A•B1***]. The formation of this binary complex facilitates the reaction between **A** and **B1*** by preorganizing their reactive sites, resulting in the formation of catalytically-inert product $\mathbf{T}^{\mathbf{AB1*}}$, in which the recognition sites used to assemble **A** and **B1*** remain associated. As a consequence, $\mathbf{T}^{\mathbf{AB1*}}$ is incapable of participating in any template-directed processes. In contrast to the minimal model of self-replication where template formation can proceed *via* reaction within ternary complex [$\mathbf{A•B1•T}^{\mathbf{AB1}}$], the reaction between **A** and **B1*** within the [**A•B1***] binary complex is independent of the template ($\mathbf{T}^{\mathbf{AB1*}}$) concentration in solution—instead, reaction through this pathway depends only on the strength of the association between **A** and **B1***. Therefore, the rate of reaction between **A** and **B1*** *via* the binary complex-directed pathway is highest at the beginning of the reaction (Figure 1, bottom right), when the concentrations of **A** and **B1*** are at their highest.

On the early Earth, self-replication would have served not only as the means of transferring information to molecular progeny, but also as an amplification mechanism, raising the concentration of a particular chemical constitution significantly above the level of its competitors in the chemical mixture in which it was present. Yet, it is apparent that in the absence of pre-formed template—or an environment with sufficient stability to ensure that any template formed remains in close proximity to the reagents—replication processes cannot operate efficiently. By contrast, template-independent processes, such as the one mediated by the [**A•B1***] complex, are not limited by the template requirement of replication processes. We envisaged, therefore, that the different, yet complementary, optimum windows of operational efficiency of these two pathways could be exploited to design a system that could utilize simultaneously both the template-independent and the template-directed pathways for its formation. This dual pathway system overcomes the limitations imposed on replicators at early reaction times as a consequence of their reliance on the bimolecular reaction between the components. In the dual pathway system, the replicator would rely on the template-independent pathway, facilitated by the binary complex, for its formation. Once formed, a conformational change would occur within the product, allowing it to participate in the assembly of the ternary catalytically active complex [$\mathbf{A•B1•T}^{\mathbf{AB1}}$] (Figure 1) required for self-replication. We envisioned that for such a system, capable of encoding multiple reactivity modes, evolutionary pressures on the early Earth might have resulted over time in the loss of such vestigial binary complex-directed reactivity, once it was no longer necessary for its original purpose.

In order to implement this dual pathway strategy, it is necessary to merge the functionalities of the original building blocks **B1** and **B1*** (Figure 1). The new substrate, **B2** (Figure 2), must possess two recognition sites, both of which are complementary to the recognition site present in **A**. One recognition site is tailored specifically to facilitate reaction through the [**A•B2**] binary complex (*i.e.*, the template-independent pathway), leading to the formation of $\mathbf{T^{AB2*}}$ at a rate that is significantly greater than that of the bimolecular reaction. The equilibrium between $\mathbf{T^{AB2*}}$ and $\mathbf{T^{AB2}}$ allows this entity to make its recognition sites available for association with substrates **A** and **B2**. Consequently, additional $\mathbf{T^{AB2}}$ can be formed through the autocatalytic pathway facilitated by reaction within the ternary complex [$\mathbf{A•B2•T^{AB2}}$] (*i.e.*, the template-directed self-replication pathway). The key difference between conformers $\mathbf{T^{AB2*}}$ and $\mathbf{T^{AB2}}$ is the arrangement of their recognition sites with respect to each other.

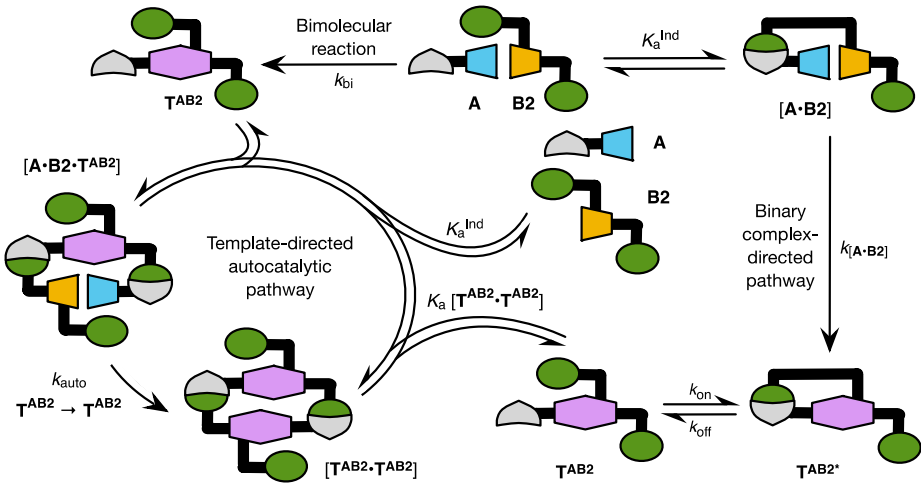


**Figure 2.** Cartoon representation of a dual pathway replicating system capable of exploiting multiple recognition-mediated reactivity modes for its formation. In this system, components **A** and **B2** are equipped with complementary recognition (gray/green) and reactive (blue/orange) sites that permit the formation of template $\mathbf{T^{AB2}}$ through a slow bimolecular reaction and a template-directed self-replication cycle. In addition, **B2** possesses an additional, yet structurally identical, recognition site (green) that permits the formation of $\mathbf{T^{AB2*}}$ through the [**A•B2**] binary complex-directed pathway. In this system, unlike that shown in Figure 1, $\mathbf{T^{AB2*}}$ is not catalytically inert since it is in equilibrium with its conformer $\mathbf{T^{AB2}}$—a self-replicating template that possesses two complementary recognition sites in an orientation that enables it to catalyze its own formation *via* template-directed reaction within a catalytically active ternary complex [$\mathbf{A•B2•T^{AB2}}$].

Importantly, we envisaged this type of system[14] would be capable of "kickstarting" the template-directed autocatalytic formation of itself by creating template through the binary complex-directed pathway at early time points in the reaction—a period when the template in replicating systems is formed exclusively *via* the slow bimolecular pathway. The resulting template, although not formed *via* the template-directed pathway, will possess all of the

recognition and reaction sites necessary to allow it to participate in the template-directed autocatalytic cycle.

Here, we report the design and characterization of a system capable of reacting through template-independent and template-dependent pathways simultaneously both experimentally and computationally. We demonstrate that the availability of both reactivity modes within the system has a positive influence on the formation of the replicating template when compared to systems that possess only one reactivity mode. Using kinetic simulations, we identify the parameter space in which a system capable of reacting through template-independent and template-dependent pathways simultaneously can operate most effectively.

**Molecular Design**

The efficiency of binary complex- and template-directed processes is dependent on the selection of appropriate complementary reaction and recognition elements. Previously, we have exploited[9d–g,12,15] a 1,3-dipolar cycloaddition reaction between a maleimide and a nitrone, and hydrogen-bonding recognition between carboxylic acids and amidopyridines for the construction of a variety of systems capable of templating their own formation[9d–g,12,16] or that of a reciprocal[15] partner. In order to implement the design shown schematically in Figure 2, we identified a set of four compounds (Figure 3)—one maleimide (**A**) and three nitrones (**B1**, **B1***, and **B2**), equipped with complementary[17] carboxylic acid and amidopyridine recognition sites.

These compounds allow us to characterize the kinetic behavior of the system capable of exploiting both the template-directed autocatalytic and the binary complex-directed pathway for its formation, as well as the two systems capable of exploiting only one of these recognition-mediated pathways for their formation—against which we could calibrate the performance of the system capable of exploiting both pathways simultaneously. The reaction between maleimide **A** and nitrone **B1** (Figure 3a) is based on a molecular framework that has been shown[9d,f,g,12] previously to be an efficient replicating system and was selected as a platform to examine the template-directed pathway in isolation. Analogously, the reaction between maleimide **A** and nitrone **B1*** was designed to characterize the efficiency of the [**A•B1***] binary complex-directed pathway in isolation (Figure 3b). Guided by electronic structure calculations, the nitrone attachment points in **B1*** have been reversed relative to **B1** in this system in order to promote reactivity through the binary complex-directed pathway. Finally, the reaction between maleimide **A** and nitrone **B2**—now bearing two amidopyridine recognition sites, one

on either side of the nitrone reactive site—was designed to investigate the kinetic behavior of the replicating system capable of operating through both the binary complex-directed and the template-directed pathways (Figure 3c). Each of the three nitrones, **B1**, **B1***, and **B2**, was designed to carry a non-polar nonynyl group (or two nonynyl groups in the case of **B2**) for enhanced solubility in $CDCl_3$.

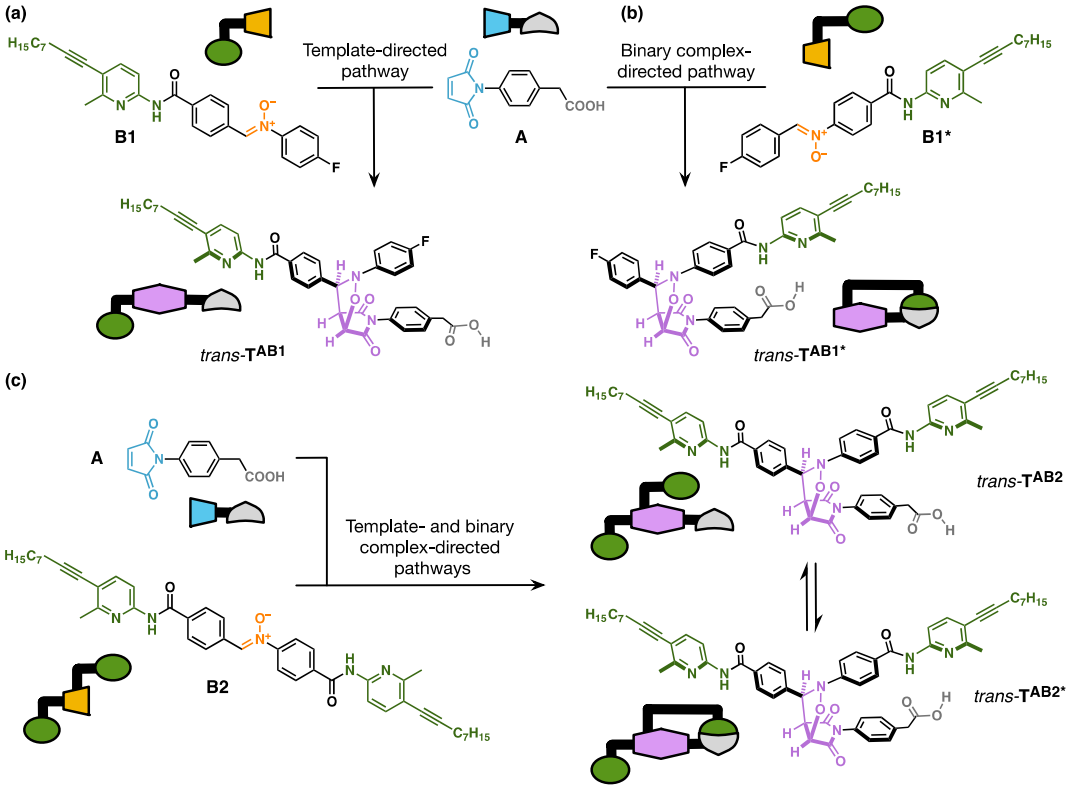


**Figure 3.** (a) A phenylacetic acid maleimide building block **A** can react with nitrone **B1**, bearing a 5-nonyne-6-methylamidopyridine recognition site, to form template *trans*-$\mathbf{T^{AB1}}$. This template possesses both of the recognition sites derived from **A** and **B1** in an open orientation that enable it to template its own formation *via* the formation of catalytically active ternary complex [**A•B1•***trans*-$\mathbf{T^{AB1}}$]. (b) Maleimide **A** can also react with nitrone **B1***, in which the nitrone attachment points are reversed compared to those in nitrone **B1**. This reaction proceeds *via* a binary complex ([**A•B1***]) directed pathway to afford template *trans*-$\mathbf{T^{AB1*}}$, in which the two recognition sites are in close proximity, rendering it catalytically inactive. (c) Reaction of maleimide **A** with nitrone **B2**, which possesses two 5-nonyne-6-methylamidopyridine recognition sites, can proceed through both the template-directed autocatalytic pathway (*via* [**A•B2•***trans*-$\mathbf{T^{AB2}}$]) and the [**A•B2**] binary complex-directed pathway, to produce *trans*-$\mathbf{T^{AB2}}$ and *trans*-$\mathbf{T^{AB2*}}$, respectively, which exist in an equilibrium.

We performed electronic structure calculations at the ωB97X/def2-SVP level of theory and a continuum solvation model for $CHCl_3$ in order to assess the viability of the key transition states in this system. The recognition-mediated cycloadditions—either templated or template-independent—between **A** and either **B1** or **B2** are designed in such a way that they should both afford only one of the two diastereoisomeric[18] products, namely the *trans* isomer (Figure 4). Our calculations demonstrate clearly that plausible transition states leading to *trans*

cycloadducts are accessible from both the [**A•B1•***trans*-**T**$^{\mathbf{AB1}}$] ternary complex (Figure 4a) and binary complex [**A•B1***] (Figure 4b). Interestingly, the transition state that is accessible from the [**A•B1***] complex does not possess the expected hydrogen-bonded dyad normally associated[9e,12c,d,15a,19] with the interaction between an amidopyridine and a carboxylic acid. Instead, a single hydrogen bond is present between the acid proton of **A** and the pyridine ring nitrogen of **B1***. It is possible that this sub-optimal recognition geometry may have an adverse effect on the reactivity of this binary complex.

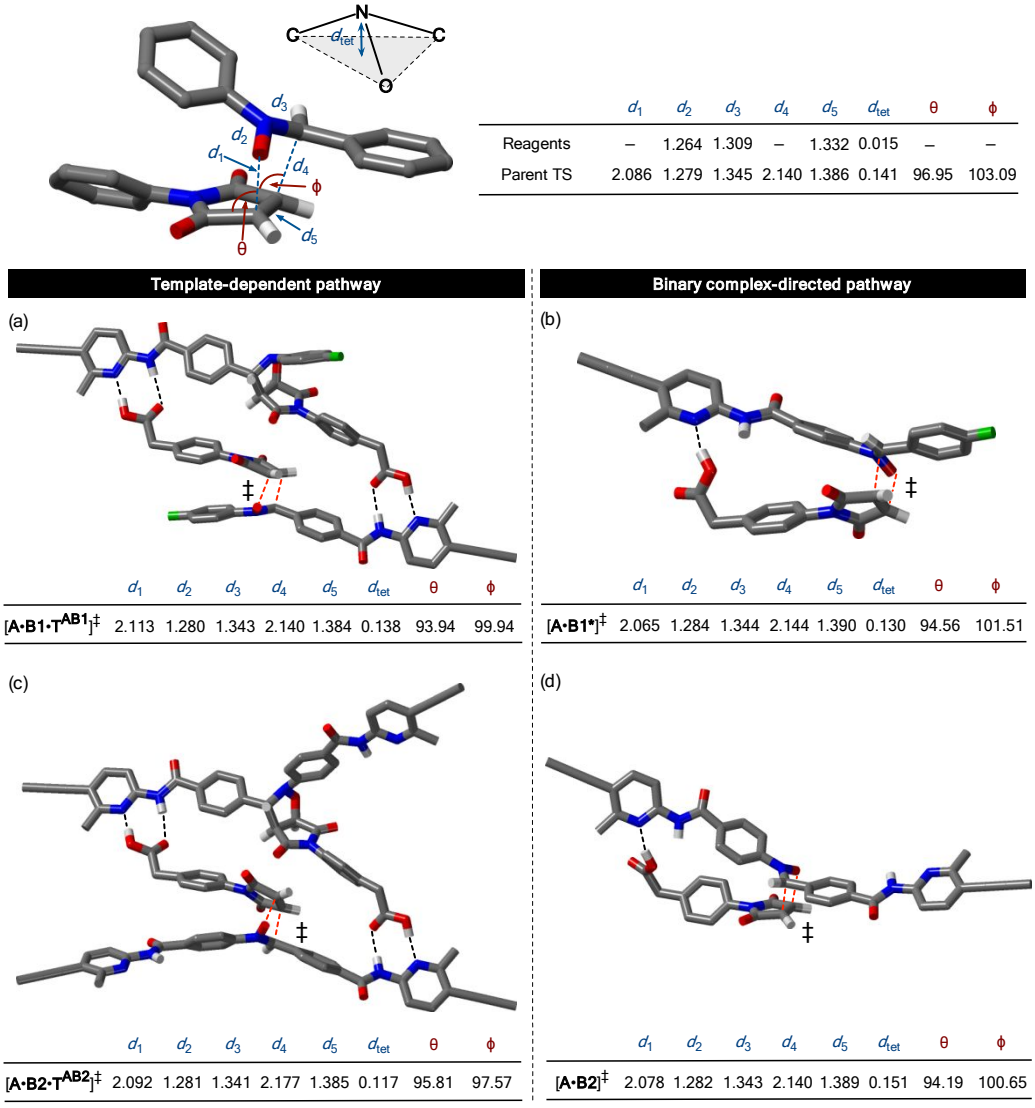


| | $d_1$ | $d_2$ | $d_3$ | $d_4$ | $d_5$ | $d_{tet}$ | θ | ϕ |
|---|---|---|---|---|---|---|---|---|
| Reagents | – | 1.264 | 1.309 | – | 1.332 | 0.015 | – | – |
| Parent TS | 2.086 | 1.279 | 1.345 | 2.140 | 1.386 | 0.141 | 96.95 | 103.09 |

| | $d_1$ | $d_2$ | $d_3$ | $d_4$ | $d_5$ | $d_{tet}$ | θ | ϕ |
|---|---|---|---|---|---|---|---|---|
| [**A•B1•T**$^{\mathbf{AB1}}$]$^{‡}$ | 2.113 | 1.280 | 1.343 | 2.140 | 1.384 | 0.138 | 93.94 | 99.94 |
| [**A•B1***]$^{‡}$ | 2.065 | 1.284 | 1.344 | 2.144 | 1.390 | 0.130 | 94.56 | 101.51 |
| [**A•B2•T**$^{\mathbf{AB2}}$]$^{‡}$ | 2.092 | 1.281 | 1.341 | 2.177 | 1.385 | 0.117 | 95.81 | 97.57 |
| [**A•B2**]$^{‡}$ | 2.078 | 1.282 | 1.343 | 2.140 | 1.389 | 0.151 | 94.19 | 100.65 |

**Figure 4.** (a) Calculated structures of the transition states (‡) accessed by (a) [**A•B1•***trans*-**T**$^{\mathbf{AB1}}$], (b) [**A•B1***], (c) [**A•B2•***trans*-**T**$^{\mathbf{AB2}}$], and (d) [**A•B2**]. Calculations were performed at the ωB97X/def2-SVP level of theory using the polarized continuum solvation model for chloroform. Hydrogen bonds are represented using dashed black lines and partial bonds in transition states using dashed red lines. Carbon atoms are colored gray, nitrogen atoms blue, oxygen atoms red, fluorine atoms green, and hydrogen atoms white. Most hydrogen atoms are omitted for clarity. Nonynyl groups were replaced by propynyl groups in the calculations in order to reduce computational resource requirements. Data for the corresponding parameters for the transition state located for the reaction of diphenylnitrone and *N*-phenyl maleimide are provided at the top of the figure for comparison (data taken from Ref. 12d). All distances are in Å, and angles are in degrees.

The operation of the network described in Figure 2, in which the binary complex [**A•B2**] generates *trans*-$\mathbf{T^{AB2}}$ through reaction and conformational change, thereby kickstarting reaction through ternary complex [**A•B2•***trans*-$\mathbf{T^{AB2}}$], relies on both of the transition states described in Figure 4a and 4b being accessible simultaneously from nitrone **B2**. Pleasingly, electronic structure calculations at the ωB97X/def2-SVP level of theory (Figure 4c and 4d) were able to locate two transition states leading to the *trans* cycloadducts from complexes of nitrone **B2**. The ternary complex [**A•B2•***trans*-$\mathbf{T^{AB2}}$] can access a transition state (Figure 4c) leading to the [*trans*-$\mathbf{T^{AB2}}$•*trans*-$\mathbf{T^{AB2}}$] duplex that is almost identical in structure to that located for the [**A•B1•***trans*-$\mathbf{T^{AB1}}$] ternary complex (Figure 4a). Similarly, reaction of **A** with **B2** within the [**A•B2**] complex affords *trans*-$\mathbf{T^{AB2*}}$, and the transition state located for this process (Figure 4d) is almost identical in structure to that located for the model system shown in Figure 4b.

In summary, these calculations indicate that the reactions of **A** with both **B1** and **B1*** should afford the *trans* diastereoisomer preferentially. Consequently, the reaction of maleimide **A** with the nitrone **B2**, which merges the structures of **B1** and **B1*** within a single entity, should similarly afford the *trans* diastereoisomer selectively—this cycloadduct is accessible through both a template-directed pathway (*via* [**A•B2•***trans*-$\mathbf{T^{AB2}}$]) and a binary complex-directed template-independent pathway (*via* [**A•B2**]).

## Results and Discussion

With the chemical building blocks required to test the viability of the reaction pathways shown schematically in Figure 2 and in terms of chemical structures in Figure 3 identified successfully, we could proceed with evaluating their efficiencies experimentally. To this end, we first examined the pairwise reactions of each **B1** and **B1*** with maleimide **A**, as well as its recognition-disabled counterpart, $\mathbf{A^{OMe}}$, in which the carboxylic acid was protected as its methyl ester. In each kinetic experiment, an equimolar solution of the desired reagents was prepared in $CDCl_3$ at 20 mM, and the progress of their reaction at 273 K was assayed at intervals of 30 minutes by 500.1 MHz $^1$H NMR spectroscopy for 16 h. The concentrations of the product species in solution could be determined at each time point by deconvolution (see Supporting Information) of the appropriate resonances in the range $\delta_H$ 4.0 to 6.0 arising from the fused bicyclic ring system present in the $\mathbf{T^{AB1}}$ and $\mathbf{T^{AB1*}}$ cycloadducts, as well as their recognition-disabled counterparts $\mathbf{T^{AOMeB1}}$ and $\mathbf{T^{AOMeB1*}}$.

As expected, the reaction between nitrone **B1** and recognition-disabled maleimide $\mathbf{A}^{\mathbf{OMe}}$ (Figure 5a, black circles) proceeded slowly and with poor diastereoselectivity.[20] After 16 h, the *trans* and *cis* diastereoisomers were formed at concentrations of 1.54 mM and 0.41 mM ([*trans*]:[*cis*] ratio = 3.8:1), respectively, reaching a combined conversion of 9.7%. By contrast, the reaction of nitrone **B1** with recognition-enabled maleimide **A** (Figure 5b, large filled green circles) under the same conditions resulted in a strikingly different reaction profile—*trans*-$\mathbf{T}^{\mathbf{AB1}}$ is formed rapidly and reaches a concentration of 15.4 mM after 16 h. The other diasteroisomer, *cis*-$\mathbf{T}^{\mathbf{AB1}}$, is formed at a considerably slower rate, reaching a concentration of 0.15 mM after the same time. Overall, after 16 h, 78% of **A** and **B1** are converted into cycloadducts and the [*trans*]:[*cis*] ratio is 106:1.

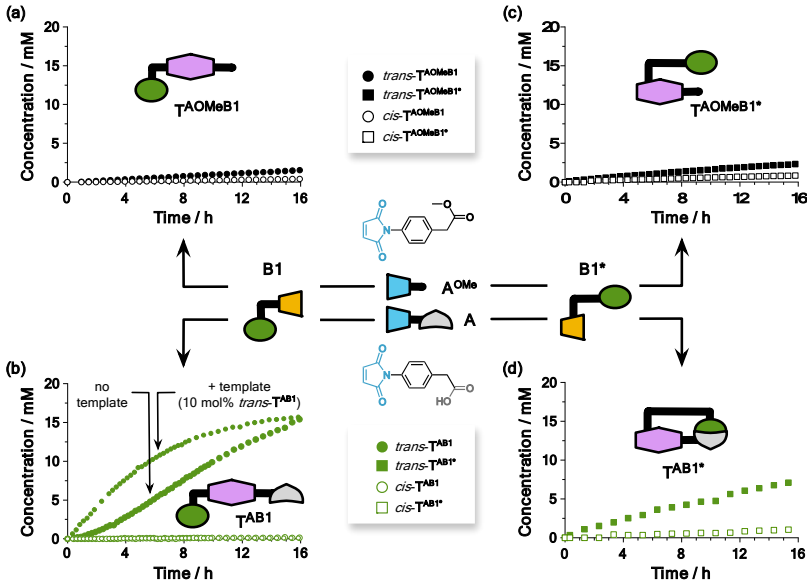


**Figure 5.** Kinetic experiments examining the reaction of nitrone **B1** with (a) recognition-disabled maleimide $\mathbf{A}^{\mathbf{OMe}}$ and (b) recognition-enabled maleimide **A**, and nitrone **B1*** with (c) recognition-disabled maleimide $\mathbf{A}^{\mathbf{OMe}}$ and (d) recognition-enabled maleimide **A** to form *trans* (filled symbols) and *cis* (empty symbols) diastereoisomeric products of (a) $\mathbf{T}^{\mathbf{AOMeB1}}$, (b) $\mathbf{T}^{\mathbf{AB1}}$, (c) $\mathbf{T}^{\mathbf{AOMeB1*}}$, and (d) $\mathbf{T}^{\mathbf{AB1*}}$, as determined by 500.1 MHz $^1$H NMR spectroscopy. Reaction conditions: $CDCl_3$, [**B1**] or [**B1***] = [$\mathbf{A}^{\mathbf{OMe}}$] or [**A**] = 20 mM, 273 K. (b) Formation of replicator *trans*-$\mathbf{T}^{\mathbf{AB1}}$ was examined in the absence (large green circles) and in the presence of 10 mol% of preformed template of *trans*-$\mathbf{T}^{\mathbf{AB1}}$ (small green circles); the concentrations of *trans*-$\mathbf{T}^{\mathbf{AB1}}$ have been corrected for the amount of template added.

In addition, the concentration *vs.* time profile for the formation of *trans*-$\mathbf{T}^{\mathbf{AB1}}$ exhibits a sigmoidal shape, which is often associated with, and sometimes displayed by, self-replicating systems. In order to verify the ability of this molecular framework to template its own formation, we repeated the experiment monitoring the formation of $\mathbf{T}^{\mathbf{AB1}}$ from its constituent components in the presence of preformed 10 mol% of *trans*-$\mathbf{T}^{\mathbf{AB1}}$, added at $t$ = 0. The time–

course profile (Figure 5b, small filled green circles) obtained for this template-instructed reaction revealed the disappearance of the lag period, thus confirming that *trans*-$\mathbf{T^{AB1}}$ retains its ability to self-replicate. In this kinetic experiment, *trans*-$\mathbf{T^{AB1}}$ and *cis*-$\mathbf{T^{AB1}}$ reached concentrations of 15.7 mM and 0.12 mM, respectively, after 16 h ([*trans*]:[*cis*] ratio = 131:1).

Having confirmed the ability of *trans*-$\mathbf{T^{AB1}}$ to template its own formation, we wished to establish the ability of $\mathbf{T^{AB1*}}$ to form *via* the [**A•B1***] binary complex-directed pathway. In order to gain insight into the bimolecular reaction between these components, nitrone **B1*** was first reacted with control maleimide $\mathbf{A^{OMe}}$ (Figure 5c, black squares). After 16 h, the *trans* and *cis* diastereoisomeric products were formed at 2.3 mM and 0.85 mM ([*trans*]:[*cis*] ratio = 2.8:1), respectively, with a combined conversion of 16%. The reaction of nitrone **B1*** with maleimide **A** (Figure 5d, green squares) under the same conditions, however, afforded *trans*-$\mathbf{T^{AB1*}}$ at a concentration of 7.1 mM. Additionally, *cis*-$\mathbf{T^{AB1*}}$ was formed[21] at a considerably slower rate, reaching a concentration of only 1.04 mM over the same time period. Overall, after 16 h, 41% of **A** and **B1*** were converted into products ([*trans*]:[*cis*] = 6.8:1). In this case, the presence of the recognition sites engendered a more modest increase in the rate of formation of *trans*-$\mathbf{T^{AB1*}}$ (*via* binary complex-directed pathway) than that observed for *trans*-$\mathbf{T^{AB1}}$ (*via* template-directed pathway), although the effect on the reaction rate associated with the presence of the [**A•B1***] complex was unambiguous.

Using two model nitrones—**B1** and **B1***—each bearing a single recognition site, we were able to characterize the kinetics of the two recognition-mediated pathways in isolation. In the next step, we set out to investigate the kinetic behavior of the system combing the recognition site features specific to nitrones **B1** and **B1*** within a single building block—nitrone **B2**. As before, we examined first the reaction of nitrone **B2** with the recognition-disabled maleimide $\mathbf{A^{OMe}}$ (Figure 6a, black diamonds). The time–course for this reaction revealed that it proceeds slowly and with low diastereoselectivy; after 16 h, *trans*-$\mathbf{T^{AOMeB2}}$ was produced at a concentration of only 1.43 mM, while *cis*-$\mathbf{T^{AOMeB2}}$ was produced at a concentration of 0.48 mM. Overall, only 9.6% of the starting materials were converted to products ([*trans*]:[*cis*] ratio = 3:1). The impact of the recognition processes on this system was investigated by examining the reaction of nitrone **B2** with maleimide **A**. In this case, the concentration *vs.* time profile (Figure 6b, pale purple diamonds) revealed the selective formation of the *trans*-$\mathbf{T^{AB2}}$ cycloadduct at 17.3 mM. By contrast, the concentration of *cis* cycloadduct reached only[22] 1.1 mM after 16 h ([*trans*]:[*cis*] ratio = 16:1). The concentration *vs.* time profile for the formation of *trans*-$\mathbf{T^{AB2}}$ displays a

sigmoidal shape, but with a significantly shorter lag period than that observed in the time–course profile of the self-replicating system bearing a single amidopyridine recognition site only (Figure 5b, *trans*-$\mathbf{T^{AB1}}$).

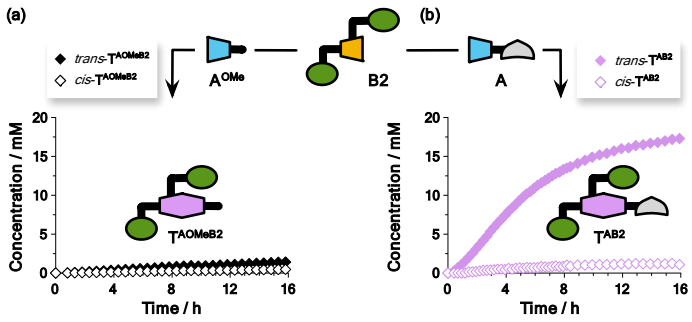


**Figure 6.** Kinetic experiments examining the reaction of nitrone **B2**, bearing two amidopyridine recognition sites, with (a) recognition-disabled maleimide $\mathbf{A^{OMe}}$ and (b) recognition-enabled maleimide **A** to form *trans* (filled symbols) and *cis* (empty symbols) diastereoisomeric products of (a) $\mathbf{T^{AOMeB2}}$ and (b) $\mathbf{T^{AB2}}$ as determined by 500.1 MHz $^1$H NMR spectroscopy. Reaction conditions: $CDCl_3$, [$\mathbf{A^{OMe}}$] or [**A**] = [**B2**] = 20 mM, 273 K.

In order to establish whether the product *trans*-$\mathbf{T^{AB2}}$ has the capacity to exploit the autocatalytic pathway, we examined the reaction between nitrone **B1** and maleimide **A** in the presence of 10 mol% of preformed template *trans*-$\mathbf{T^{AB2}}$. As described previously, the reaction progress was monitored by 500.1 MHz $^1$H NMR spectroscopy over a period of 16 h. The resulting time course (Figure S2a) shows that the addition of preformed template *trans*-$\mathbf{T^{AB2}}$ at $t$ = 0 h removes the lag period, in a manner similar to that observed in the reaction instructed with preformed *trans*-$\mathbf{T^{AB1}}$. This result demonstrates that the two building blocks, **A** and **B1**, each bearing a single recognition site, can be pre-organized on the template *trans*-$\mathbf{T^{AB2}}$ in a co-conformation that facilitates their reaction, enabling efficient formation of *trans*-$\mathbf{T^{AB1}}$ even early in the reaction time course. Although this observation suggests that *trans*-$\mathbf{T^{AB2}}$ is capable of exploiting the template-directed pathway for its formation, we wished to demonstrate further that the observed effect is related to the presence of the recognition sites required for self-replication and not those mediating product formation *via* the binary complex-directed pathway. To this end, we examined the reaction of nitrone **B1** and maleimide **A** in the presence of 10 mol% of preformed template *trans*-$\mathbf{T^{AB1*}}$, formed by the reaction of **A** and **B1*** *via* the [**A•B1***] binary complex-directed pathway. We reasoned that, unlike the addition of preformed *trans*-$\mathbf{T^{AB2}}$, the presence of this template should exert no effect on the formation of *trans*-$\mathbf{T^{AB1}}$. Examination of the time–course obtained for this reaction (Figure S2b) revealed that, as expected, there is no noticeable difference between the rates of production of template *trans*-$\mathbf{T^{AB1}}$ with or without *trans*-$\mathbf{T^{AB1*}}$. These findings demonstrate that *trans*-$\mathbf{T^{AB1*}}$—the product

formed *via* the [**A•B1***] binary complex-directed pathway—is not able to act as a template for the reaction between nitrone **B1** and maleimide **A**.

In order to better understand the impact of combining the various recognition sites into a single molecular framework, we compared the kinetic time–course profiles obtained for the system *via* the binary complex-directed pathway (Figure 7, labeled AB only; reaction of **A** with **B1***), the system operating *via* the template-directed self-replication pathway (Figure 7, labeled SR only; reaction of **A** with **B1**), and the full system exploiting both the binary complex- and template-directed pathways (Figure 7, labeled AB and SR; reaction of **A** with **B2**). Comparison of the overall efficiencies, as determined by the final concentrations of *trans* products formed in each kinetic experiment, revealed that the system capable of exploiting both recognition pathways (Figure 7, pale purple diamonds) produces the *trans* template most effectively, followed by the system operating *via* the template-directed pathway (Figure 7, green circles) and, finally, by the system operating *via* the binary-complex-directed pathway (Figure 7, green squares).

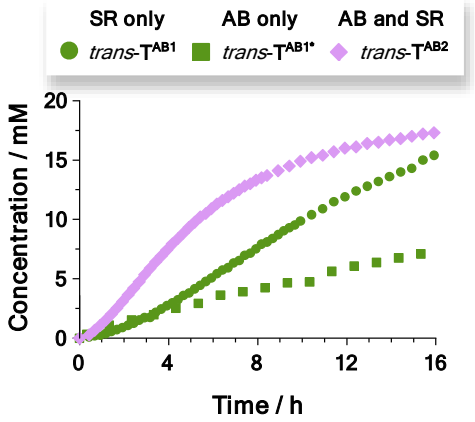


**Figure 7.** Reaction profiles showing the production of *trans* diastereoisomer *via* the template-directed self-replication pathway (SR only; green circles), the binary complex-directed pathway (AB only; green squares), and the system capable of exploiting both binary complex- and template-directed pathways (AB and SR; pale purple diamonds) over 16 h.

In order to compare the efficiencies of these three systems, especially in the first 25% of the reaction time course, we calculated the rate[23] *vs* time profiles (Figure S4) corresponding to the time courses shown in Figure 7. From these rate profiles, we determined the average rate of template formation over the first 4 h of reaction for each system (*i.e.*, *the* first 25% of the reaction time course; for details, see the Supporting Information S3.4). Comparison of these average rate values revealed that the system capable of exploiting both recognition-mediated pathways (*trans*-$\mathbf{T^{AB2}}$ exploits both AB and SR) displays the highest rate of 2.1 mM $h^{-1}$ within

the 0 to 4 h time window. By contrast, the systems operating *via* the binary complex-directed pathway or the template-directed pathway only reached a rate of 0.55 mM $h^{-1}$ (*trans*-$\mathbf{T^{AB1*}}$; AB only) and 0.81 mM $h^{-1}$ (*trans*-$\mathbf{T^{AB1}}$**;** SR only), respectively. These results indicate that the replicator constructed from nitrone **B2**, which bears two recognition sites, takes advantage of both the binary complex channel *and* the template-directed autocatalytic channel to fabricate itself more rapidly during the first 25% of the reaction time course—a period during which self-replicators are typically very inefficient as a result of their initial reliance on the bimolecular pathway for their formation.

Having demonstrated the ability of the system bearing one carboxylic acid and two amidopyridine recognition sites to exploit both reactivity modes effectively, we now wished to examine the possibility of utilizing (Figure 8a) the accelerated *in situ* formation of template *trans*-$\mathbf{T^{AB2}}$, as a means of kickstarting the self-replication of template *trans*-$\mathbf{T^{AB1}}$. To this end, we performed an experiment in which the reaction of nitrone **B1** with maleimide **A** was carried out in the presence of a small quantity of nitrone **B2**, bearing two amidopyridine recognition sites. Specifically, a reaction mixture containing **B1** at 20 mM, **A** at 24 mM, and **B2** at 4 mM (*i.e.*, 20 mol% relative to the concentration of **B1**) was prepared in $CDCl_3$ and the reaction progress was monitored by 500.1 MHz $^1$H NMR spectroscopy at 273 K (Figure 8b, filled gray circles). We envisaged that nitrone **B2** will be able to react with maleimide **A** to produce template *trans*-$\mathbf{T^{AB2}}$ more rapidly at early time points in the reaction through the template-independent, binary complex-directed pathway (*i.e.*, *via* complex [**A•B2**]). Once formed, the *trans*-$\mathbf{T^{AB2}}$ template present in solution will catalyze not only the reaction between nitrone **B1** and maleimide **A** (*via* [**A•B2•***trans*-$\mathbf{T^{AB2}}$]) but also the reaction between nitrone **B1** with maleimide **A** to afford *trans*-$\mathbf{T^{AB1}}$ (Figure 8, *via* [**A•B1•***trans*-$\mathbf{T^{AB2}}$], kickstart pathway). Therefore, the formation of template *trans*-$\mathbf{T^{AB2}}$, capable of exploiting two recognition-directed pathways for its formation, serves as an *in situ* catalyst for the production of *trans*-$\mathbf{T^{AB1}}$. Consequently, the formation of *trans*-$\mathbf{T^{AB1}}$ proceeds at an increased rate relative to its formation in the situation where the increased concentration of 24 mM is employed for all components, but nitrone **B2** is absent (*i.e.*, conditions where formation of *trans*-$\mathbf{T^{AB2}}$ is not possible; Figure 8b, filled black circles).

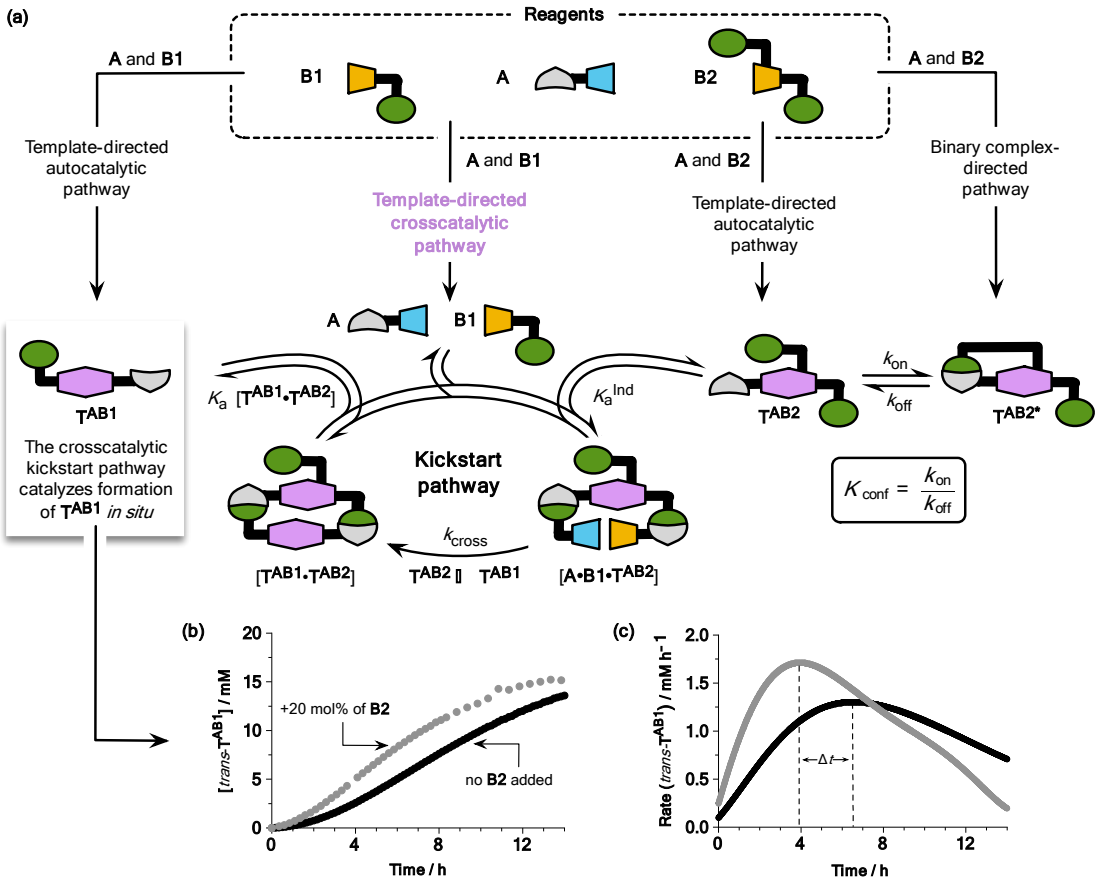


**Figure 8.** (a) Cartoon representation of a reaction network assembled from maleimide **A** and nitrones **B1** and **B2**, showing the recognition-mediated pathways through which these components can react. The presence of **B2** enables *in situ* formation of template *trans*-$\mathbf{T^{AB2}}$ *via* two recognition-mediated pathways. Once formed, *trans*-$\mathbf{T^{AB2}}$ kickstarts the self-replication of template *trans*-$\mathbf{T^{AB1}}$ *via* an otherwise unavailable crosscatalytic pathway (pale purple). In the absence of *trans*-$\mathbf{T^{AB2}}$, the formation of *trans*-$\mathbf{T^{AB1}}$ would rely on the slow, bimolecular pathway early on in the time course (see Figure 1). (b) Concentration and (c) rate *vs.* time profiles for the formation of *trans*-$\mathbf{T^{AB1}}$ from nitrone **B1** and maleimide **A** in the absence (black; [**A**] = [**B1**] = 24 mM) of nitrone **B2**, bearing two amidopyridine recognition sites, and in the presence of **B2** (gray, +20 mol% relative to **A**; [**A**] = 24 mM, [**B1**] = 20 mM, [**B2**] = 4 mM), in $CDCl_3$, as determined at 273 K by 500.1 MHz $^1$H NMR spectroscopy.

A comparison of the concentration *vs.* time profiles obtained in the presence and absence of nitrone **B2** (Figure 8b, filled gray *vs.* filled black circles, respectively) reveals that the production of template *trans*-$\mathbf{T^{AB1}}$ is accelerated in the presence of nitrone **B2**, equipped with two amidopyridine recognition sites. The effect of the presence of *trans*-$\mathbf{T^{AB2}}$ on the formation of *trans*-$\mathbf{T^{AB1}}$ is exposed[24] most readily by examining the rate *vs.* time profiles[23] for these reactions (Figure 8c, gray *vs.* black lines). When **B2** is present (and, therefore, *trans*-$\mathbf{T^{AB2}}$ is also formed in the reaction mixture), there is a significant increase in the rate of formation of *trans*-$\mathbf{T^{AB1}}$ (Figure 8c, gray) and the maximum rate occurs at an earlier time point (maximum rate of 1.71 mM h$^{-1}$ at $t$ = 4.0 h). By contrast, when **B2** is absent in the reaction mixture (Figure 8c, black), the maximum rate of formations of *trans*-$\mathbf{T^{AB1}}$ is 1.30 mM h$^{-1}$ and this maximum

occurs later in the course of the reaction ($t$ = 6.6 h). These observations are characteristic of the effect of the addition of an instructional template on the formation of a replicator. These results demonstrate conclusively that the autocatalytic cycle leading to the formation of replicator *trans*-$\mathbf{T^{AB1}}$ can be instructed by the presence of template *trans*-$\mathbf{T^{AB2}}$ in the system, even when *trans*-$\mathbf{T^{AB2}}$ is formed *in situ*.

## Kinetic fitting and simulations

The comprehensive set of kinetic experiments presented in the previous section has validated the design and operation of the two recognition-mediated pathways in this system—the template-independent pathway, mediated by the [**A•B2**] binary complex, and the template-directed autocatalytic pathway, operating through the ternary, catalytically active complex ([**A•B2•***trans*-$\mathbf{T^{AB2}}$]). In order to develop a better understanding of the kinetic behavior of such systems operating through both of these recognition-mediated pathways, and the contributions of each individual pathway to the overall performance, we fitted the reaction time courses shown in Figures 5 and 6 to the appropriate kinetic models (for fitting protocols, see Section S3.2 in the Supporting Information). We were able to determine the rate and stability constants (Table S1) associated with the bimolecular and recognition-mediated 1,3-dipolar cycloaddition reactions in the three systems designed to probe the efficiency of the binary complex-directed pathway, the template-directed pathway, or both of these pathways operating within a single framework. Through this process of kinetic fitting, we were able to establish the kinetic effective molarity[25,26] ($EM_{kinetic}$) associated with each recognition-mediated pathway in isolation. The value of $EM_{kinetic}$ for the system capable of exploiting the binary complex-directed pathway (**A** + **B1***, data in Figure 5d) was determined to be 0.082 M (82 mM). This value is consistent with the modest increase in reactivity observed for the reaction between **A** and **B1*** at 20 mM in $CDCl_3$, at 273 K, when compared to the corresponding reaction of **B1*** with recognition-disabled maleimide $\mathbf{A^{OMe}}$. By contrast, the system capable of exploiting the template-directed pathway for its formation (**A** + **B1**, data in Figure 5b) exhibited a markedly higher value of $EM_{kinetic}$ of 15.3 M. Comparison of these values of $EM_{kinetic}$ for the two recognition-mediated pathways in isolation indicates that the template-directed pathway is significantly more efficient—by a factor of almost 200—than the binary complex-directed pathway at producing the corresponding *trans* diastereoisomeric product.

With these data in hand, we were able to assess the efficiency of the system encoding multiple recognition-mediated reactivity modes. The kinetic model describing the dual pathway system incorporates an additional parameter describing the key conformational equilibrium—characterized by an equilibrium constant termed $K_{conf}$[27] (Figure 8a). This parameter is a measure of the proportion of species present in the open (*trans*-$\mathbf{T^{AB2}}$) and the closed (*trans*-$\mathbf{T^{AB2*}}$) conformations of the product formed by the reaction of maleimide **A** and nitrone **B2** (data in Figure 6b). In the kinetic model, the lower the value of $K_{conf}$, the higher the proportion of the *trans* diastereoisomer present in the open configuration required for participation in the template-directed pathway. The simultaneous fitting of the three key parameters—rate constants $k_{[A•B2]}$ and $k_{auto}$, and $K_{conf}$—afforded values of $EM_{kinetic}$ of 0.316 M (template-independent) and 21.0 M (template-dependent) for the two recognition-mediated pathways, respectively. Both of these values are somewhat higher than the corresponding values for the recognition-mediated pathways determined in isolation (Table S1). The best fit of the kinetic model to the experimental data was obtained using a value of $K_{conf}$ of 17 (for details, see Table S2). Any fitting attempts employing a value of $K_{conf}$ of less than 15 made no significant changes to the quality of the fit. It appears, therefore, that once a critical concentration of the open form of template—*trans*-$\mathbf{T^{AB2}}$—is reached, its availability stops being rate-limiting in the reaction network.

In order to better comprehend the relative contributions of the two recognition-mediated pathways to the formation of the *trans* product, we developed a simulation model based on the kinetic model used in parameter fitting. Using this model, we simulated the outcome of the system encoding multiple reactivity modes employing the fitted parameters (Table S1). This kinetic simulation allowed us to examine the relative concentrations of all components and complexes in our experimental system as a function of time. Importantly, we could therefore determine the flux through each recognition-mediated pathway by calculating the rates associated with the binary complex-directed pathway ($k_{[A•B2]} \times$ [**A•B2**]; labeled as $r_{AB}$) and the template-directed self-replication pathway ($k_{auto} \times$ [**A•B2•***trans*-$\mathbf{T^{AB2}}$]; labeled as $r_{SR}$) at each time point (Figure 9). By calculating the $log_{10}$ of the ratio $r_{SR}/r_{AB}$ (Figure 9a), we can reveal time periods where the template-independent pathway is dominant ($log_{10}(r_{SR}/r_{AB}) < 0$) and time periods where the template-dependent pathway is dominant ($log_{10}(r_{SR}/r_{AB}) > 0$). Thus, in the experimental system (Figure 9), up to around 1.7 h, the binary complex-directed pathway contributes more significantly than the template-directed pathway to the formation of *trans*-$\mathbf{T^{AB2}}$. However, a transition point occurs around 1.7 h, when the template-directed

pathway starts to dominate. Hence, the results of the kinetic simulation shown in Figure 9 suggest that the system designed in this work to encode multiple reactivity modes benefits considerably from the template-independent, binary complex-directed pathway at the beginning of the reaction. The flux of material through this recognition-mediated pathway allows the system to produce significant amounts of *trans*-$\mathbf{T^{AB2}}$ in the time period 0 to 2 h when, typically, self-replicating systems exhibit very limited efficiency.

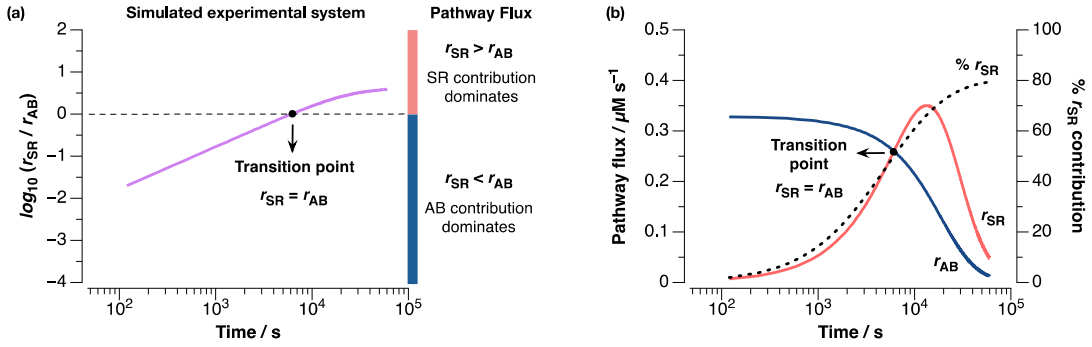


**Figure 9.** Simulated relative contributions of the binary complex-directed pathway (labeled AB) and the template-directed self-replication pathway (labeled SR) to product formation in the experimental system encoding multiple reactivity modes. The relative contributions of the two recognition-mediated pathways were determined by calculating the flux through each pathway ($r_{AB} = k_{[A•B2]} \times$ [**A•B2**]; $r_{SR} = k_{auto} \times$ [**A•B2**•*trans*-$\mathbf{T^{AB2}}$]) as a function of time. (a) The dashed line represents the boundary (at $log_{10}(r_{SR}/r_{AB}) = 0$) between the regime in which the binary complex-directed pathway (blue area) dominates and the regime dominated by the template-directed pathway (red area). (b) The flux through the two pathways (left axis) as a function of time and the proportion of the template-directed self-replication (SR) pathway to the overall formation of *trans*-$\mathbf{T^{AB2}}$ as a percentage of the total flux ($r_{AB} + r_{SR}$) through the recognition-mediated pathways (right axis).

The results of simulations shown in Figure 9 reveal the relative contributions of the two recognition-mediated pathways to product formation in the system examined experimentally, and are, thus, associated with a single, specific molecular design. In order to examine how the simultaneous operation of two recognition-mediated pathways affects the performance of self-replicating systems more generally, we performed three additional sets of simulations. In these three sets of simulations, we examined the changes in the relative contributions of the template-independent binary complex-directed pathway (Figure 10, labeled AB) and the template-directed self-replication pathway (Figure 10, labeled SR) as a function of $K_{conf}$ (0.1, 10, and 1000, Figure 10a–c). Within each simulation set, we varied the efficiencies of the two recognition-mediated pathways—examining two scenarios where both pathways operate either with low efficiency (Figure 10, black = slow) or high efficiency (Figure 10, orange = fast), and two scenarios where only one of the recognition-mediated pathways operates efficiently (Figure 10, green and gray). The results of these additional simulations revealed several key patterns of behavior. First, the template-directed pathway contributes significantly to product

formation only when the equilibrium between the open (*i.e.*, catalytically active) and closed (*i.e.*, catalytically inactive) configurations of the template lies sufficiently far to the side of the open form (*i.e.*, $K_{conf}$ = 0.1 and 10, Figure 10a and 10b). By contrast, if the template is present predominantly in the closed form (*i.e.*, $K_{conf}$ = 1000, Figure 10c), the binary complex-directed pathway remains the dominant recognition-mediated pathway at all times simulated (*i.e.*, the transition point is not observed within the simulated timeframe). Second, the relative contributions of the two recognition-mediated pathways to product formation are directly linked to their relative and absolute efficiencies. In all simulated scenarios at $K_{conf}$ = 0.1 and 10, in which the binary complex-directed pathway is the only recognition-mediated pathway operating efficiently (Figure 10a and 10b, gray), the contribution of the binary complex-directed pathway to product formation exceeds that of the template-directed pathway at all times examined. In comparison, the simulated scenarios in which both pathways operate with relatively low or high efficiencies (Figure 10a and 10b, black and orange) show increased relative contribution of the template-directed pathway to overall product formation.

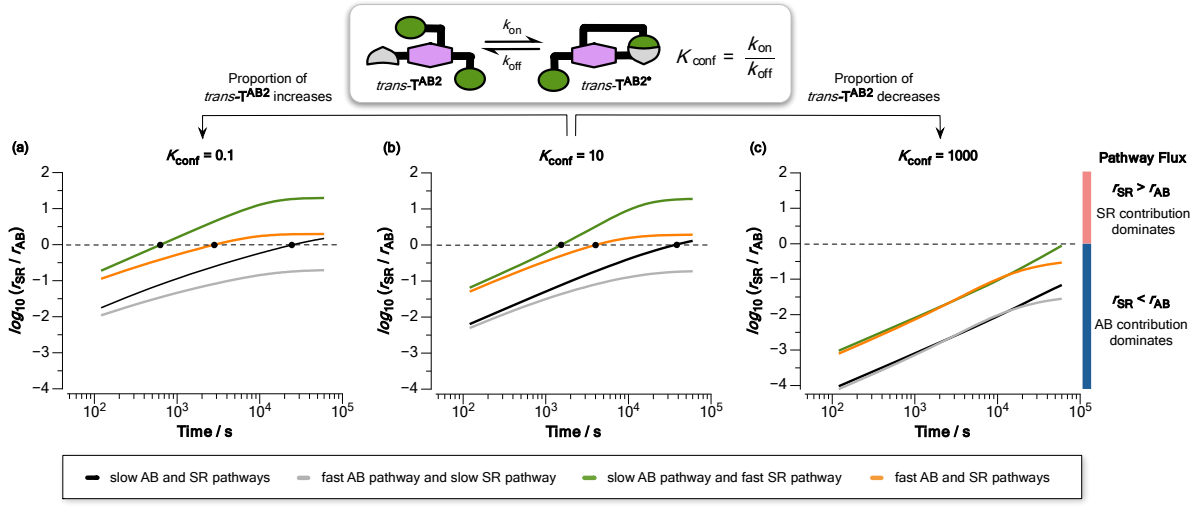


**Figure 10.** (a–c) Simulated relative contributions of the binary complex-directed pathway (labeled AB) and the template-directed self-replication pathway (labeled SR) to product formation in theoretical systems encoding multiple reactivity modes. The relative contributions of the two recognition-mediated pathways were determined by calculating the flux through each pathway ($r_{AB} = k_{[A•B2]} \times$ [**A•B2**]; $r_{SR} = k_{auto} \times$ [**A•B2•***trans*-$\mathbf{T^{AB2}}$]) as a function of time and values of $K_{conf}$ (a: 0.1; b: 10; c: 1000) and $EM_{kinetic}$. Note that the terms slow and fast are relative and represent different values of $EM_{kinetic}$ for each type of recognition-mediated pathway (see Table S3 for details). In each plot, the dashed line represents the boundary (at $log_{10}(r_{SR}/r_{AB}) = 0$) between the regime in which the binary complex-directed pathway (blue area, $log_{10}(r_{SR}/r_{AB}) < 0$) dominates and the regime dominated by the template-directed pathway (red area, $log_{10}(r_{SR}/r_{AB}) > 0$) and the points of transition are marked with black dots where necessary.

The optimum scenario—that is, a situation where the binary complex-directed pathway dominates only early on in the reaction, and is followed by a transition (Figure 10, black dots) to a regime where the template-directed pathway provides the dominant contribution to product

formation—is observed most closely in simulations where only the template-directed pathway operates efficiently (Figure 10a and 10b, green). In such an optimum scenario, there is both a sufficient amount of catalytically active template produced at early stages of the reaction, and the duration of the reaction phase that permits efficient information transfer (*i.e.*, product formation *via* the template-directed pathway) is maximized. Our simulations demonstrate that such an optimum system requires the parameter $K_{conf}$ to be as low as possible, and for the template-directed pathway to be significantly more efficient than the template independent pathway.

Overall, it is clear that there is a particular set of conditions that allow a replicating system to benefit from the operation of a binary complex-directed pathway. The experimental system examined in this work—characterized by a rather inefficient binary complex-directed pathway and efficient template-directed pathway, in combination with a sufficient quantity of template present in the open form—matches these conditions. As a result, the interplay between the two complementary recognition-mediated reactivity modes in the replicating system has a positive influence on product formation in the replicating system when compared to systems capable of operating through a single recognition-mediated reactivity mode only.

## Conclusions

In this work, we have described the rational design and experimental implementation of a template, *trans*-$\mathbf{T^{AB2}}$, that is capable of managing its own replication through the simultaneous operation of a conventional template-directed autocatalytic pathway and a template-independent recognition-mediated pathway. We have established using a comprehensive set of kinetic experiments, simulations and analyses, that, at least in the system reported here, the template-independent pathway, mediated by the [**A•B2**] complex, plays a critical role at early time points in the reaction. During this period early in the time course of the reaction, the efficiency of conventional template-directed autocatalytic replication is diminished considerably as a result of the inherently low concentration of the replicating template. In this system, the template-independent pathway produces a significant concentration of the replicating template *trans*-$\mathbf{T^{AB2}}$ during the initial stages of the reaction. Hence, the conventional template-directed autocatalytic replication pathway can establish itself much earlier in the time course of the reaction than would be the case in the absence of the additional template-independent pathway. We have demonstrated that this approach can also be used in a

crosscatalytic sense, where the *in situ* formation of *trans*-$\mathbf{T^{AB2}}$ can be used to initiate and accelerate the formation of the complementary conventional replicator *trans*-$\mathbf{T^{AB1}}$.

The recognition-mediated reactivity through two pathways that is encoded within the design of *trans*-$\mathbf{T^{AB2}}$ has significant attractions. However, kinetic simulations suggest that the parameter space within which these two pathways can operate successfully in concert is relatively small. In this context, the successful operation of a system exploiting this dual pathway approach is a situation in which almost all the reaction flux passes through the conventional template-directed autocatalytic replication pathway after a short initial period during which the template independent pathway is dominant. Our kinetic simulations suggest that systems, such as the one reported here, can be expected to operate successfully with the following combination of parameters: The critical conformational equilibrium that connects the two recognition-mediate pathways, between the open conformation (*trans*-$\mathbf{T^{AB2}}$) and its closed counterpart (*trans*-$\mathbf{T^{AB2*}}$) and which is characterized by $K_{conf}$, must be such that at least 1 to 2% ($K_{conf} < \sim 20$) is of the template is present in the open form. In addition, the relative efficiency of the template-directed autocatalytic replication pathway with respect to the template independent pathway must be such that the ratio of the effective molarities for reaction within the respective reactive complexes ([**A•B2•***trans*-$\mathbf{T^{AB2}}$] and [**A•B2**]) is significantly more than 20.

The system reported here represents a proof-of-concept study in which we have successfully engineered a synthetic replicating system that is capable of profiting from multiple productive formation pathways by virtue of its enhanced interactional capabilities that are encoded within the replicator components. Given the restrictions on the parameter space within which a replicator can benefit from this enhanced functionality, it is unlikely that this type of system is of significant relevance to the emergence of simple organic replicators on the early Earth. However, this concept may be of more relevance to replicators which lie at connection points between two replicator networks. Their capacity to receive and pass instructions between different functional reaction networks using combinations of their multiple recognition sites could allow such templates to function as the interconnects necessary to generate more complex network architectures. Establishing sound design parameters for the encoding of multiple reaction pathways within a single replicator therefore represents a key objective for systems chemistry research that is directed toward the development of complex interconnected reaction networks.

## Associated Content

### Supporting Information

Supporting information is available free of charge at:

General experimental procedures; synthetic procedures and compound characterization; details of kinetic analyses, fitting (including fitted kinetic profiles and example scripts), and simulations; and details of computational methods and binding constant determination.

## Author Information

### Corresponding author

*E-mail: d.philp@st-andrews.ac.uk

### ORCID ID

Craig C. Robertson: 0000-0002-1419-9618

Tamara Kosikova: 0000-0001-7886-9660

Douglas Philp: 0000-0002-9198-4302

### Present Address

†(C.C.R.) Department of Chemistry, University of Sheffield, Brook Hill, Sheffield S3 7HF, United Kingdom

## Notes

The authors declare no competing financial interest.

## Acknowledgements

Financial support for this work was provided by the University of St Andrews and EaStCHEM, Northwestern University, and the Engineering and Physical Sciences Research Council (Grant EP/K503162/1).

## References and Notes


1. (a) Frenkel-Pinter, M.; Samanta, M.; Ashkenasy, G.; Leman, L. J. Prebiotic peptides: molecular hubs in the origin of life. *Chem. Rev.* **2020**, DOI: 10.1021/acs.chemrev.9b00664. (b) Xavier, J. C.; Hordijk, W.; Kauffman, S.; Steel, M.; Martin, W. F. Autocatalytic chemical networks at the origin of metabolism. *Proc. R. Soc. B* **2020**, *287*, 20192377. (c) Ritson, D. J.; Battilocchio, C.; Ley, S. V.; Sutherland, J. Mimicking the surface and prebiotic chemistry of early Earth using flow chemistry. *Nat. Commun.* **2018**, *9*, 1921. (d) Sutherland, J. D. Opinion: studies on the origin of life—the end of the beginning. *Nat. Rev. Chem.* **2017**, *1*, 0012. (e) Sutherland, J. D. The origin of life—out of the blue. *Angew. Chem., Int. Ed.* **2016**, *55*, 104–121. (f) Rauchfuss, H. In: *Chemical Evolution and the Origin of Life*; Mitchell, T. N. Ed.; Springer: Berlin, 2008. (g) Luisi, P. L. *The emergence of life*; Cambridge University Press, 2006. (h) Mason, S. F. *Chemical Evolution*; Oxford University Press, Inc.: New York, 1991.
2. (a) Preiner, M.; Asche, S.; Becker, S.; Betts, H. C.; Boniface, A.; Camprubi, E.; Chandru, K.; Erastova, V.; Garg, S. G.; Khawaja, N.; Kostyrka, G.; Machné, R.; Moggioli, G.; Muchowska, K. B.; Neukirchen, S.; Peter, B.; Pichlhöfer, E.; Radványi, Á.; Rossetto, D.; Salditt, A.; Schmelling, N. M.; Sousa, F. L.; Tria, F. D. K.; Vörös, D.; Xavier, J. C. The future of origin of life research: bridging decades-old divisions. *Life* **2020**, *10*, 20. (b) Ruiz-Mirazo, K.; Briones, C.; de la Escosura, A. Prebiotic systems chemistry: new perspectives for the origins of life. *Chem. Rev.* **2014**, *114*, 285−366. (c) Mann, S. The origins of life: old problems, new chemistries. *Angew. Chem., Int. Ed.* **2013**, *52*, 155−162. (d) Neveu, M.; Kim, H.-J.; Benner, S. A. The "strong" RNA world hypothesis: fifty years old. *Astrobiology* **2013**, *13*, 391−403. (e) Lazcano, A. Historical development of origins research. *Cold Spring Harbor Perspect. Biol.* **2010**, *2*, a002089. (f) Deamer, D.; Weber, A. L. Bioenergetics and life's origins. *Cold Spring Harbor Perspect. Biol.* **2010**, *2*, a004929. (g) Peretó, J. Controversies on the origin of life. *Int. Microbiol.* **2005**, *8*, 23−31.
3. (a) Islam, S.; Powner, M. W. Prebiotic systems chemistry: complexity overcoming clutter. *Chem* **2017**, *2*, 470–501. (b) Miljanić, O. Š. Small-molecule systems chemistry. *Chem* **2017**, *2*, 502–524. (c) Ashkenasy, G.; Hermans, T. M.; Otto, S.; Taylor, A. F. Systems chemistry. *Chem. Soc. Rev.* **2017**, *46*, 2543–2554. (d) de la Escosura, A.; Briones, C.; Ruiz-Mirazo, K. The systems perspective at the crossroads between chemistry and biology. *J. Theor. Biol.* **2015**, *381*, 11−22. (e) Mattia, E.; Otto, S. Supramolecular systems chemistry. *Nat. Nanotechnol.* **2015**, *10*, 111−119. (f) Giuseppone, N. Toward self-constructing materials: A systems chemistry approach. *Acc. Chem. Res.* **2012**, *45*, 2178–2188.
4. (a) Inoue, T.; Joyce, G. F.; Grzeskowiak, K.; Orgel, L. E.; Brown, J. M.; Reese, C. Template-directed synthesis on the pentanucleotide CpCpGpCpC. *J. Mol. Biol.* **1984**, *178*, 669–676. (b) Inoue, T.; Orgel, L. E. A nonenzymatic RNA polymerase model. *Science* **1983**, *219*, 859–862. (c) Lohrmann, R.; Orgel, L. E. Efficient catalysis of polycytidylic acid-directed oligoguanylate

formation by $Pb^{2+}$. *J. Mol. Biol.* **1980**, *142*, 555–567. (d) Orgel, L. E.; Lohrman, R. Prebiotic chemistry and nucleic acid replication. *Acc. Chem. Res.* **1974**, *7*, 368–377.

5. von Kiedrowski, G. A self-replicating hexadeoxynucleotide. *Angew. Chem., Int. Ed. Engl.* **1986**, *25*, 932–935.
6. (a) Duim, H.; Otto, S. Towards open-ended evolution in self-replicating molecular systems. *Beilstein J. Org. Chem.* **2017**, *13*, 1189−1203. (b) Kosikova, T.; Philp, D. Exploring the emergence of complexity using synthetic replicators. *Chem. Soc. Rev.* **2017**, *46*, 7274–7305. (c) Bissette, A. J.; Fletcher, S. P. Mechanisms of autocatalysis. *Angew. Chem., Int. Ed.* **2013**, *52*, 12800–12826. (d) Philp, D.; Huck, J. Supramolecular Chemistry: From Molecules to Nanomaterials; John Wiley & Sons, Ltd.: New York, 2012; Vol. 4, pp. 1415–1445. (e) Vidonne, A.; Philp, D. Making molecules make themselves—the chemistry of artificial replicators. *Eur. J. Org. Chem.* **2009**, 593–610. (f) Dadon, Z.; Wagner, N.; Ashkenasy, G. The road to non-enzymatic molecular networks. *Angew. Chem., Int. Ed.* **2008**, *47*, 6128–6136. (g) Patzke, V.; von Kiedrowski, G. Self-replicating systems. *ARKIVOC* **2007**, *46*, 293–310. (h) Paul, N.; Joyce, G. F. Minimal self-replicating systems. *Curr. Opin. Chem. Biol.* **2004**, *8*, 634–639. (i) Von Kiedrowski, G. Minimal replicator theory I: parabolic versus exponential growth. *Bioorganic Chem. Front.* **1993**, *3*, 113–146.
7. For examples of minimal synthetic self-replicators based on oligonucleotides, see: (a) Plöger, T. A.; von Kiedrowski, G. A self-replicating peptide nucleic acid. *Org. Biomol. Chem.* **2014**, *12*, 6908−6914. (b) Paul, N.; Joyce, G. F. A self-replicating ligase ribozyme. *Proc. Natl. Acad. Sci. U. S. A.* **2002**, *99*, 12733−12740. (c) Luther, A.; Brandsch, R.; von Kiedrowski, G. Surface-promoted replication and exponential amplification of DNA analogues. *Nature* **1998**, *396*, 245–248. (d) Achilles, T.; von Kiedrowski, G. A self-replicating system made from three starting materials. *Angew. Chem., Int. Ed. Engl.* **1993**, *32*, 1198–1201. (e) von Kiedrowski, G.; Wlotzka, B.; Helbing, J.; Matzen, M.; Jordan, S. Parabolic growth of a self-replicating hexadeoxynucleotide bearing a 3′-5′-phosphoamidate linkage. *Angew. Chem., Int. Ed. Engl.* **1991**, *30*, 423−426.
8. For examples of minimal synthetic self-replicators based on peptides, see: (a) Colomb-Delsuc, M.; Mattia, E.; Sadownik, J. W.; Otto, S. Exponential self-replication enabled through a fibre elongation/breakage mechanism. *Nat. Commun.* **2015**, *6*, 7427. (b) Samiappan, M.; Dadon, Z.; Ashkenasy, G. Replication NAND gate with light as input and output. *Chem. Commun.* **2011**, *47*, 710−712. (c) Carnall, J. M. A.; Waudby, C. A.; Belenguer, A. M.; Stuart, M. C. A.; Peyralans, J. J.-P.; Otto, S. Mechanosensitive self-replication driven by self-organization. *Science* **2010**, *327*, 1502−1506. (d) Issac, R.; Chmielewski, J. Approaching exponential growth with a self-replicating peptide. *J. Am. Chem. Soc.* **2002**, *124*, 6808−6809. (e) Saghatelian, A.; Yokobayashi, Y.; Soltani, K.; Ghadiri, M. R. A chiroselective peptide replicator. *Nature* **2001**, *409*, 797−801. (f) Lee, D. H.; Granja, J. R.; Martinez, J. A.; Severin, K.; Ghadiri, M. R. A self-replicating peptide. *Nature* **1996**, *382*, 525−528.

9. For examples of minimal synthetic self-replicators based on small organic molecules, see: (a) Morrow, S. M.; Colomer, I.; Fletcher, S. P. A chemically fueled self-replicator. *Nat. Commun.* **2019**, *10*, 1011. (b) Colomer, I.; Morrow, S. M.; Fletcher, S. P. A transient self-assembling self-replicator. *Nat. Commun.* **2018**, *9*, 2239. (c) Taylor, J. W.; Eghtesadi, S. A.; Points, L. J.; Cronin, L. Autonomous model protocell division driven by molecular replication. *Nat. Commun.* **2017**, *8*, 237. (d) Bottero, I.; Huck, J.; Kosikova, T.; Philp, D. A synthetic replicator drives a propagating reaction−diffusion front. *J. Am. Chem. Soc.* **2016**, *138*, 6723−6726. (e) Vidonne, A.; Kosikova, T.; Philp, D. Exploiting recognition-mediated assembly and reactivity in [2]rotaxane formation. *Chem. Sci.* **2016**, *7*, 2592−2603. (f) Sadownik, J. W.; Philp, D. A simple synthetic replicator amplifies itself from a dynamic reagent pool. *Angew. Chem., Int. Ed.* **2008**, *47*, 9965−9970. (g) Kassianidis, E.; Philp, D. Design and implementation of a highly selective minimal self-replicating system. *Angew. Chem., Int. Ed.* **2006**, *45*, 6344−6348. (h) Kindermann, M.; Stahl, I.; Reimold, M.; Pankau, W. M.; von Kiedrowski, G. Systems chemistry: kinetic and computational analysis of a nearly exponential organic replicator. *Angew. Chem., Int. Ed.* **2005**, *44*, 6750−6755. (i) Wang, B.; Sutherland, I. O. Self-replication in a Diels−Alder reaction. *Chem. Commun.* **1997**, 1495− 1496. (j) Rotello, V.; Hong, J.-I.; Rebek, J., Jr Sigmoidal growth in a self-replicating system. *J. Am. Chem. Soc.* **1991**, *113*, 9422−9423. (k) Tjivikua, T.; Ballester, P.; Rebek, J., Jr. Self-replicating system. *J. Am. Chem. Soc.* **1990**, *112*, 1249−1250.

10. For examples of networks of synthetic replicators based on oligonucleotides, see: (a) Sczepanski, J. T.; Joyce, G. F. A cross-chiral RNA polymerase ribozyme. *Nature* **2014**, *515*, 440–442. (b) Robertson, M. P.; Joyce, G. F. Highly efficient self-replicating RNA enzymes. *Chem. Biol.* **2014**, *21*, 238–245. (c) Ferretti, A. C.; Joyce, G. F. Kinetic properties of an RNA enzyme that undergoes self-sustained exponential amplification. *Biochemistry* **2013**, *52*, 1227–1235. (d) Lincoln, T. A.; Joyce, G. F. Self-sustained replication of an RNA enzyme. *Science* **2009**, *323*, 1229−1232. (e) Kim, D.-E.; Joyce, G. F. Cross-catalytic replication of an RNA ribozyme. *Chem. Biol.* **2004**, *11*, 1505−1512. (f) Sievers, D.; von Kiedrowski, G. Self-replication of hexadeoxynucleotide analogues: autocatalysis versus cross-catalysis. *Chem. - Eur. J.* **1998**, *4*, 629−641.

11. For examples of networks of synthetic replicators based on peptides, see: (a) Liu, B.; Pappas, C. G.; Ottelè, J.; Schaeffer, G.; Jurissek, C.; Pieters, P. F.; Altay, M.; Marić, I.; Stuart, M. C. A.; Otto, S. Spontaneous emergence of self-replicating molecules containing nucleobases and amino acids. *J. Am. Chem. Soc.* **2020**, *142*, 4184–4192. (b) Malakoutikhah, M.; Schaeffer, G.; Santiago, G. M.; Yang, S.; Marić, I.; Otto, S. Cross-catalysis between self-replicators of different handedness. *J. Sys. Chem.* **2019**, *7*, 9–18. (c) Altay, M.; Altay, Y.; Otto, S. Parasitic behavior of self-replicating molecules. *Angew. Chem., Int. Ed.* **2018**, *139*, 10564−10568. (d) Sadownik, J. W.; Mattia, E.; Nowak, P.; Otto, S. Diversification of self-replicating molecules. *Nat. Chem.* **2016**, *8*, 264−269. (e) Dadon, Z.; Wagner, N.; Alasibi, S.; Samiappan, M.; Mukherjee, R.; Ashkenasy, G. Competition and cooperation in dynamic replication networks. *Chem. - Eur. J.* **2015**, *21*, 648−654.

(f) Dadon, Z.; Samiappan, M.; Wagner, N.; Ashkenasy, G. Chemical and light triggering of peptide networks under partial thermodynamic control. *Chem. Commun.* **2012**, *48*, 1419−1421. (g) Dadon, Z.; Wagner, N.; Ashkenasy, G. The road to non-enzymatic molecular networks. *Angew. Chem., Int. Ed.* **2008**, *47*, 6128−6138. (h) Ashkenasy, G.; Jagasia, R.; Yadav, M.; Ghadiri, M. R. Design of a directed molecular network. *Proc. Natl. Acad. Sci. U. S. A.* **2004**, *101*, 10872−10877. (i) Yao, S.; Ghosh, I.; Zutshi, R.; Chmielewski, J. Selective amplification by auto- and cross-catalysis in a replicating peptide system. *Nature* **1998**, *396*, 447−450. (j) Severin, K.; Lee, D. H.; Martinez, J. A.; Vieth, M.; Ghadiri, M. R. Dynamic error correction in autocatalytic peptide networks. *Angew. Chem., Int. Ed.* **1998**, *37*, 126−128.

12. For examples of networks of synthetic replicators based on small organic molecules, see: (a) Kosikova, T.; Philp, D. Two synthetic replicators compete to process a dynamic reagent pool. *J. Am. Chem. Soc.* **2019**, *141*, 3059–3072. (b) Huck, J.; Kosikova, T.; Philp, D. Compositional persistence in a multicyclic network of synthetic replicators. *J. Am. Chem. Soc.* **2019**, *141*, 13905–13913. (c) Sadownik, J. W.; Kosikova, T.; Philp, D. Generating system-level responses from a network of simple synthetic replicators. *J. Am. Chem. Soc.* **2017**, *139*, 17565−17573. (d) Kosikova, T.; Philp, D. A critical cross-catalytic relationship determines the outcome of competition in a replicator network. *J. Am. Chem. Soc.* **2017**, *139*, 12579−12590. (e) Kosikova, T.; Hassan, N. I.; Cordes, D. B.; Slawin, A. M. Z.; Philp, D. Orthogonal recognition processes drive the assembly and replication of a [2]rotaxane. *J. Am. Chem. Soc.* **2015**, *137*, 16074−16083. (f) Kassianidis, E.; Pearson, R. J.; Wood, E. A.; Philp, D. Designing instructable networks using synthetic replicators. *Faraday Discuss.* **2010**, *145*, 235−254.

13. (a) Kosikova, T.; Mackenzie, H.; Philp, D. Probing the limits of selectivity in a recognition-mediated reaction network embedded within a dynamic covalent library. *Chem. - Eur. J.* **2016**, *22*, 1831−1839. (b) Sadownik, J. W.; Philp, D. A recognition-mediated reaction drives the amplification within a dynamic library. *Org. Biomol. Chem.* **2015**, *13*, 10392−10401.

14. In 1990, Rebek and co-workers reported (Ref. 9k) the first example of a self-replicator constructed from small organic molecules. In this system, the authors exploited a $Et_3N$-catalyzed amide bond formation between an adenine derivative and an imide of Kemp's triacid as the strategy for template formation. Although the authors observed a rate enhancement in response to the addition of preformed template to a solution of reactants, their design did not exhibit the expected sigmoidal reaction profile. This observation was attributed to a significant contribution from a binary complex-directed pathway to overall rate of product formation. This system, although not by design, represents the first, and to the best of our knowledge, only example of a synthetic system that exploits multiple reactivity modes for its formation.

15. (a) Robertson, C. C.; Kosikova, T.; Philp, D. An environmentally responsive reciprocal replicating network. *J. Am. Chem. Soc.* **2018**, *140*, 6832−6841. (b) Kassianidis, E.; Pearson, R. J.; Wood, E. A.; Philp, D. Designing instructable networks using synthetic replicators. *Faraday Discuss.* **2010**,

*145*, 235−254. (c) Kassianidis, E.; Philp, D. Reciprocal template effects in a simple synthetic system. *Chem. Commun.* **2006**, 4072−4074.

16. Strong product duplexes are a feature of all of the minimal replicators that we have described in the literature to date. The values of $K_a^{Duplex}$ determined through kinetic fitting for our replicators are generally in the 0.5–50 × $10^6$ $M^{-1}$ range, *i.e.*, a situation where the concentration of the catalytically active ternary complex is around 50–500 μM (see Ref. 9g for a detailed analysis) under the conditions employed experimentally. Ideally, self-replicating systems would be examined at a concentration (C) that promotes the dissociation of the template duplex ($[C]_{initial} = 1/K_a^{Duplex}$). At such a low concentration, however, the formation of the catalytically active ternary complex, which is driven by the considerably smaller $K_a^{Ind}$ (~300–3000 $M^{-1}$), would be strongly disfavoured. Therefore, the optimum experimental conditions represent a balance of these two competing influences.
17. The association constant ($K_a$) for these recognition partners, determined by $^1$H NMR spectroscopic titration, is 580 $M^{-1}$ in $CDCl_3$ at 273 K (for details, see the Supporting Information Section S2).
18. The 1,3-dipolar cycloaddition reaction between a maleimide and a nitrone can result in the formation of two diastereoisomers—denoted *trans* and *cis*. The *trans* and *cis* notation refers to the relative configuration of the three protons located on the bicyclic ring structure formed in the cycloaddition reaction. In the *trans* cycloadduct, the protons derived from the maleimide are located on the opposite face of the bicyclic ring system to the proton originating from the nitrone. In the *cis* cycloadduct, the protons derived from both the maleimide and the nitrone are located on the same face of the fused ring system. In the absence of recognition-mediated processes, the *trans* to *cis* ratio is typically around 3:1.
19. (a) Goodman, M. S.; Weiss, J.; Hamilton, A. D. A self-assembling receptor for dicarboxylic acids. *Tetrahedron Lett.* **1994**, *35*, 8943–8946. (b) Garcia-Tellado, F.; Albert, J.; Hamilton, A. D. Chiral recognition of tartaric acid derivatives by a synthetic receptor. *J. Am. Soc., Chem. Commun.* **1991**, 1761–1763. (c) Garcia-Tellado, G.; Goswami, S.; Chang, S. K.; Geib, S. J.; Hamilton, A. D. Molecular recognition: a remarkably simple receptor for the selective complexation of dicarboxylic acids. *J. Am. Chem. Soc.* **1990**, *112*, 7393–7394.
20. In the absence of recognition elements, the 1,3-dipolar cycloaddition between a maleimide and nitrone proceeds with an inherently low diastereoselectivity (*trans*:*cis* = ~3:1). Consequently, the degree of diastereoselectivity in the 1,3-dipolar cycloaddition reaction between a nitrone and maleimide can be used as a tool for quantifying the effect that the presence of a recognition-mediated pathway has on the operation of a particular system.
21. The pathway through which a cycloadduct is formed encodes the stereochemistry of the resulting bicyclic system. The data in Figure 5d shows the concentration–time profile obtained for the reaction between **A** and **B1***. In this case, only the *trans* diastereoisomer can arise from a binary complex pathway, and only the *cis* diastereoisomer can arise from a template-directed

autocatalytic process. The concentration–time profiles for the *cis* diastereoisomer in Figure 5c (recognition-disabled control reaction) and Figure 5d (recognition-enabled reaction) can be overlaid, confirming that there is no possibility that a template effect is operating for this diastereoisomer since these profiles are essentially identical.

22. This reduction in diastereoselectivity arises from the fact that *trans*-$\mathbf{T^{AB2}}$ possesses two amidopyridine recognition sites. At any given time, one of these sites is engaged in the recognition-mediated reaction processes discussed in the text. However, the second site can act as a competitive inhibitor for these processes by binding any molecules bearing a carboxylic acid. The effect of competitive inhibitors on the diastereoselectivity of autocatalytic replicators has been demonstrated by our laboratory previously. See Refs. 9e and 9g, as well as in the following publications: (a) Pearson, R. J.; Kassianidis, E.; Slawin, A. M. Z.; Philp, D. Self-replication vs. reactive binary complexes—manipulating recognition-mediated cycloadditions by simple structural modifications. *Org. Biomol. Chem.* **2004**, *2*, 3434–3441. (b) Allen, V. C.; Philp, D.; Spencer, N. Transfer of stereochemical information in a minimal self-replicating system. *Org. Lett.* **2001**, *3*, 777–780.
23. The rate for each template-directed reaction ($d$[*trans*-$\mathbf{T^{AB1}}$]/$dt$ or $d$[*trans*-$\mathbf{T^{AB2}}$]/$dt$) was determined by computing the first derivative of a seventh-order polynomial fitted to the concentration *vs* time data. The rate for the binary complex-directed reaction ($d$[*trans*-$\mathbf{T^{AB1*}}$]/$dt$) was determined by computing the first derivative of a third-order polynomial fitted to the concentration *vs* time data.
24. In order to establish that the enhancement observed in the rate of formation of *trans*-$\mathbf{T^{AB1}}$ was the result of catalysis by template *trans*-$\mathbf{T^{AB2}}$, formed *in situ* by reaction of maleimide **A** and nitrone **B2**, and not the result of additional maleimide **A** (24 mM) relative to nitrone **B1** (20 mM), we also examined the reaction between nitrone **B1** at 20 mM and maleimide **A** at 24 mM in $CDCl_3$ in the absence of nitrone **B2**. The resulting time–course profile for this reaction exhibited no discernible difference in the production or selectivity for *trans*-$\mathbf{T^{AB1}}$ when compared to the reaction where **A** and **B1** were reacted in a 1:1 ratio (at a concentration of 20 mM).
25. Kinetic effective molarity ($EM_{kinetic}$) provides a measure of the enhancement in the template-directed reaction relative to the corresponding bimolecular reaction. In addition, this parameter provides information about the concentration at which the reaction would have to be performed in order for the bimolecular pathway to perform at the same efficiency as the template-directed pathway. Consequently, rate acceleration is observed in recognition-mediated systems even if the value of $EM_{kinetic}$ is < 1 M, as long as the concentration at which the reaction is performed is lower than the $EM_{kinetic}$.
26. (a) Kirby, A. J. Effective molarities for intramolecular reactions. *Adv. Phys. Org. Chem.* **1981**, *17*, 183–278. (b) Page, M. I. The energetics of neighbouring group participation. *Chem. Soc. Rev.* **1973**, *2*, 295–323. (c) Page, M. I.; Jencks, W. P. Entropic contributions to rate accelerations in

enzymatic and intramolecular reactions and the chelate effect. *Proc. Natl. Acad. Sci. U. S. A.* **1971**, *68*, 1678–1683.

27. The value of $K_{conf}$ cannot be determined readily and accurately by experimental methods as the proportion of the "open" conformation of *trans*-$\mathbf{T^{AB2}}$ is relatively small. The low occupancy of this open state makes determining its presence quantitatively by any method based on dynamic NMR spectroscopy subject to large errors.

**For Table of Contents graphic only:**

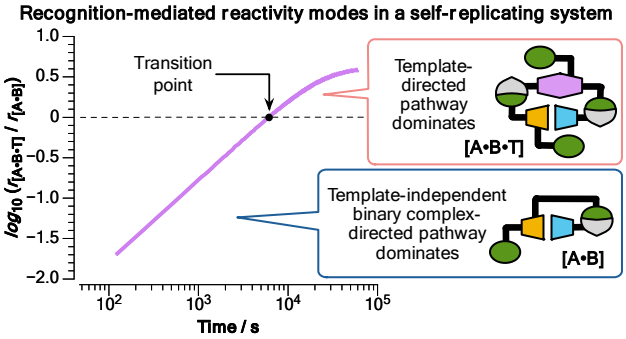

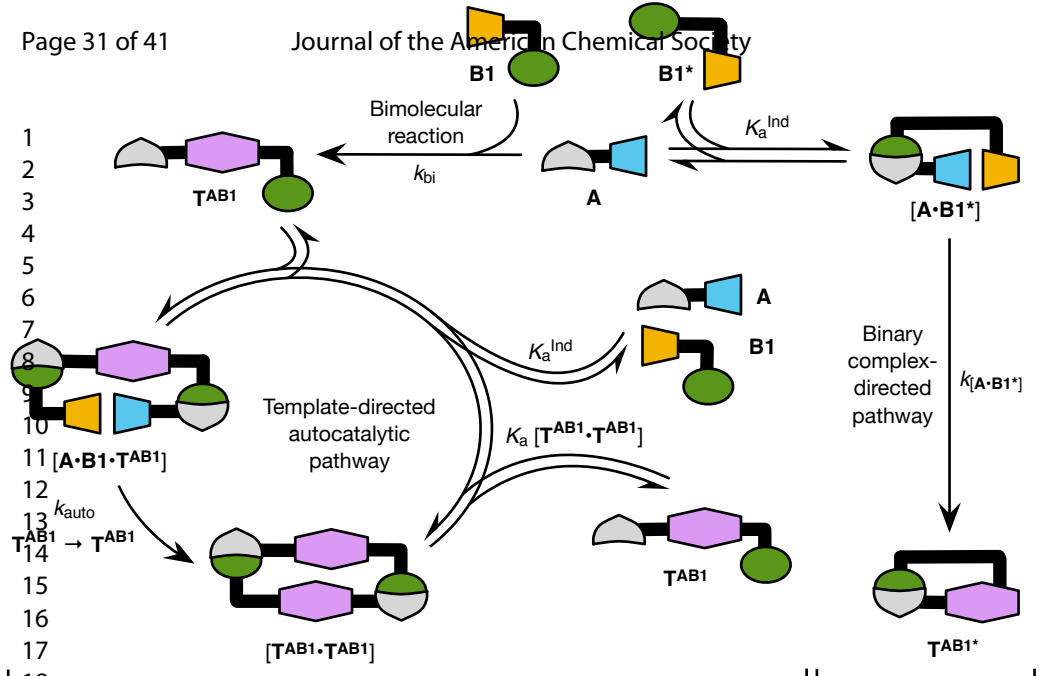


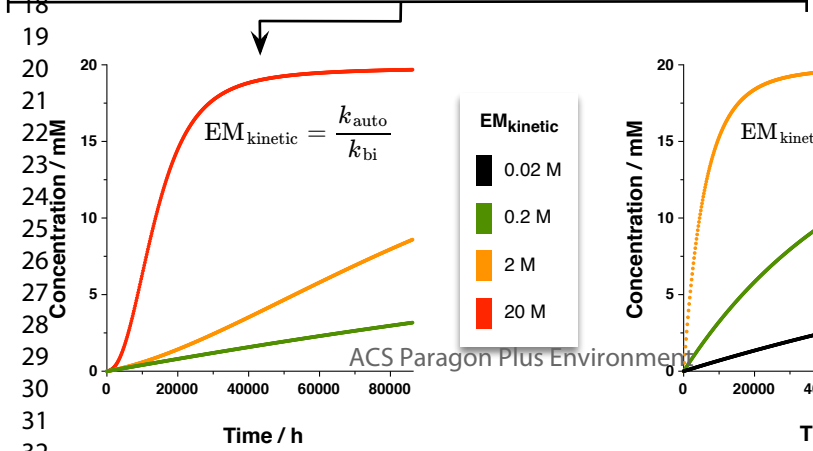

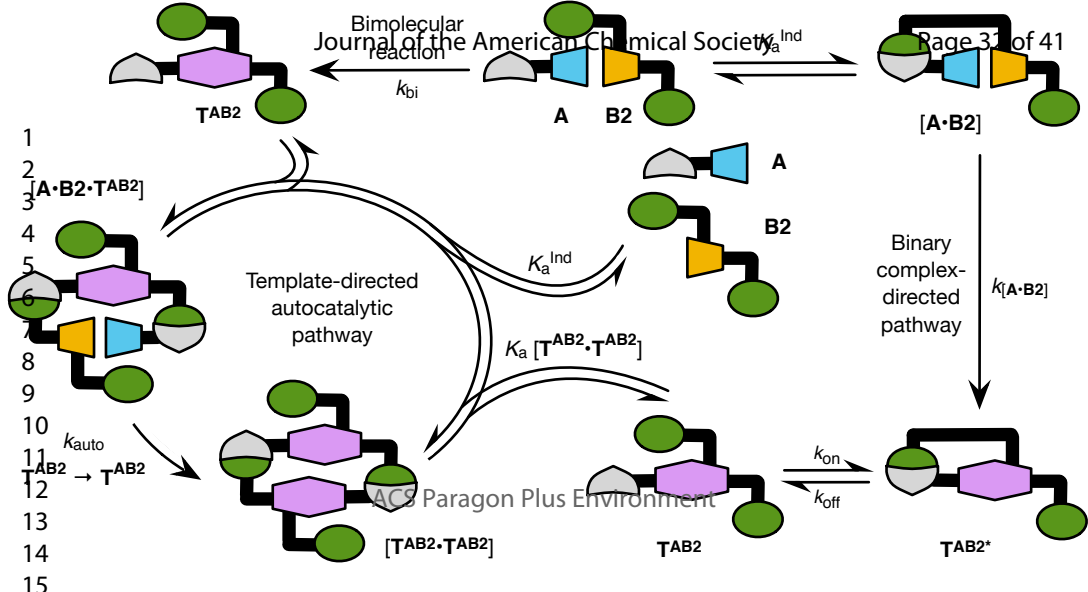

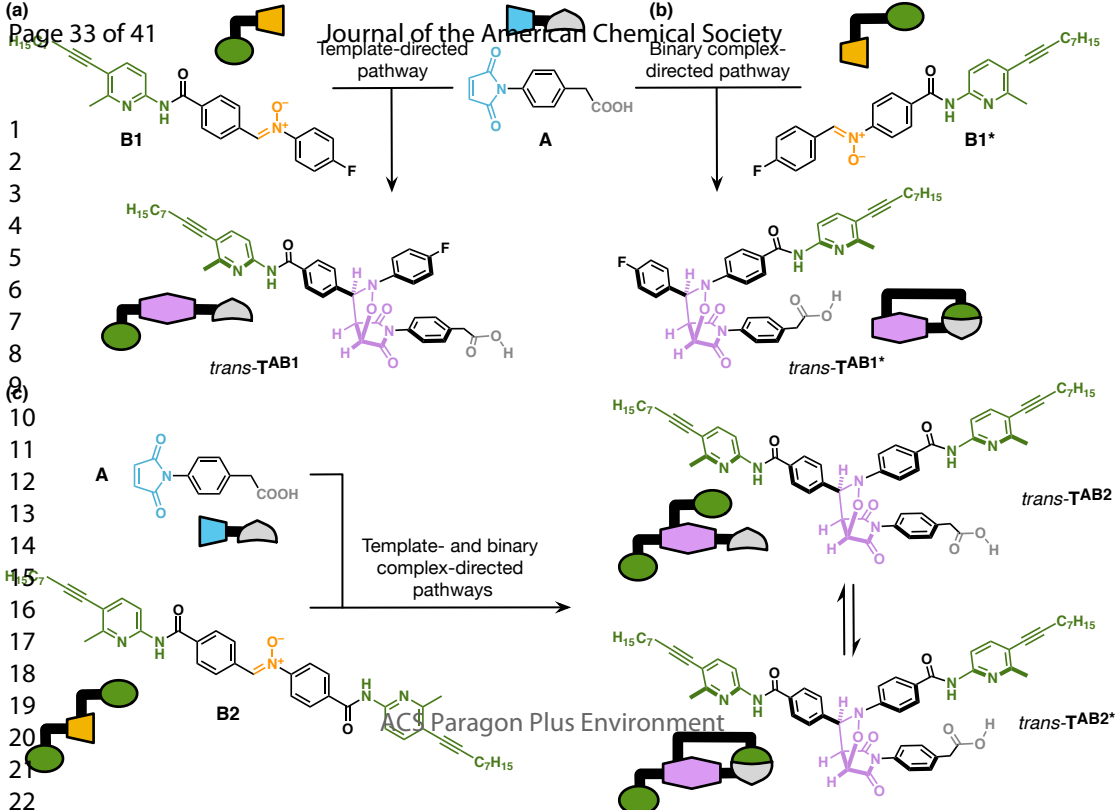

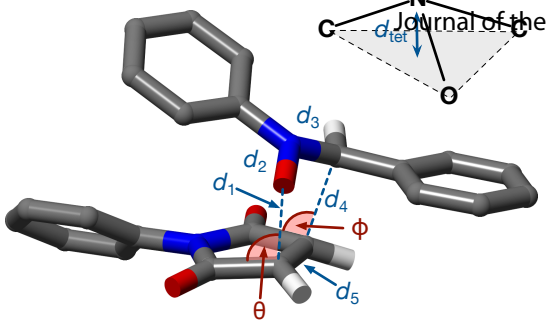


| | $d_1$ | $d_2$ | $d_3$ | $d_4$ | $d_5$ | $d_{tet}$ | θ | ϕ |
|---|---|---|---|---|---|---|---|---|
| Reagents | — | 1.264 | 1.309 | — | 1.332 | 0.015 | — | — |
| Parent TS | 2.086 | 1.279 | 1.345 | 2.140 | 1.386 | 0.141 | 96.95 | 103.09 |

**Template-dependent pathway**

(a)

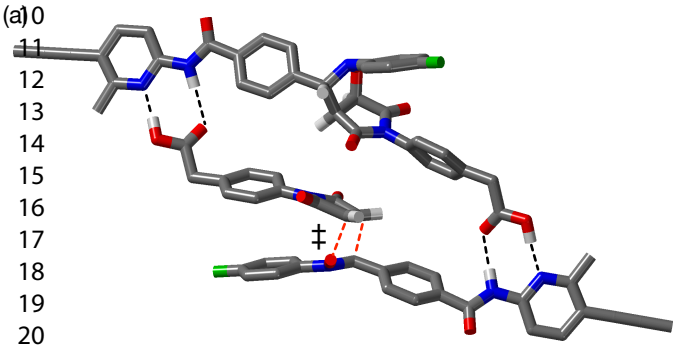

| | $d_1$ | $d_2$ | $d_3$ | $d_4$ | $d_5$ | $d_{tet}$ | θ | ϕ |
|---|---|---|---|---|---|---|---|---|
| [**A**•**B1**•**T**$^{AB1}$]‡ | 2.113 | 1.280 | 1.343 | 2.140 | 1.384 | 0.138 | 93.94 | 99.94 |

(c)

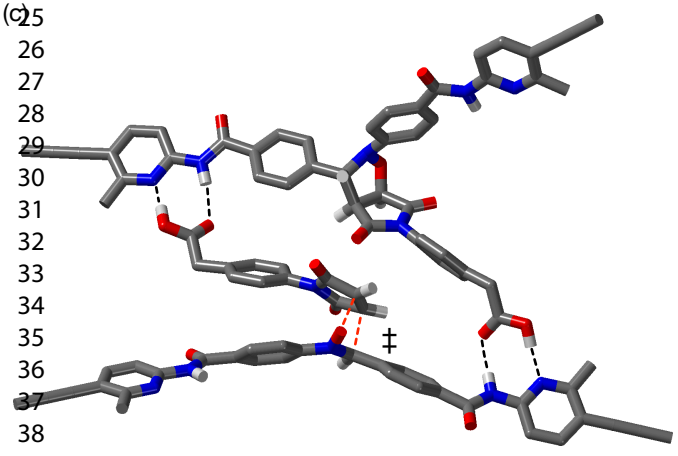

| | $d_1$ | $d_2$ | $d_3$ | $d_4$ | $d_5$ | $d_{tet}$ | θ | ϕ |
|---|---|---|---|---|---|---|---|---|
| [**A**•**B2**•**T**$^{AB2}$]‡ | 2.092 | 1.281 | 1.341 | 2.177 | 1.385 | 0.117 | 95.81 | 97.57 |

**Binary complex-directed pathway**

(b)

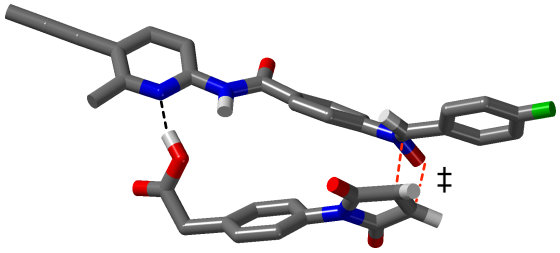

| | $d_1$ | $d_2$ | $d_3$ | $d_4$ | $d_5$ | $d_{tet}$ | θ | ϕ |
|---|---|---|---|---|---|---|---|---|
| [**A**•**B1***]‡ | 2.065 | 1.284 | 1.344 | 2.144 | 1.390 | 0.130 | 94.56 | 101.51 |

(d)

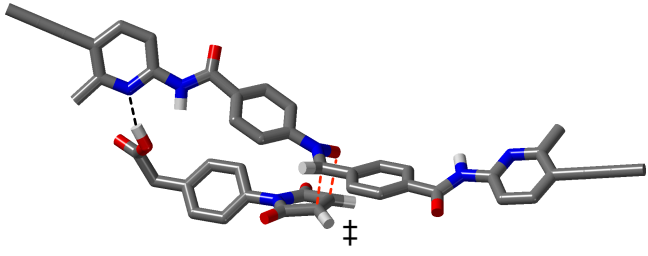

| | $d_1$ | $d_2$ | $d_3$ | $d_4$ | $d_5$ | $d_{tet}$ | θ | ϕ |
|---|---|---|---|---|---|---|---|---|
| [**A**•**B2**]‡ | 2.078 | 1.282 | 1.343 | 2.140 | 1.389 | 0.151 | 94.19 | 100.65 |